Europe PMC Funders Group
Author Manuscript
Nat Metab. Author manuscript; available in PMC 2019 November 01.

Published in final edited form as:
Nat Metab. 2019 May ; 1(5): 546–559. doi:10.1038/s42255-019-0055-6.

4-Methylumbelliferone improves the thermogenic capacity of brown adipose tissue

Maria Grandoch[1,*], **Ulrich Flögel**[2], **Sam Virtue**[3], **Julia K. Maier**[1], **Tomas Jelenik**[4,5], **Christina Kohlmorgen**[1], **Kathrin Feldmann**[1], **Yanina Ostendorf**[1], **Tamara R. Castañeda**[5,6], **Zhou Zhou**[5,6], **Yu Yamaguchi**[7], **Emmani B.M. Nascimento**[8], **Vivekananda G. Sunkari**[9], **Christine Goy**[10], **Martina Kinzig**[11], **Fritz Sörgel**[11], **Paul L. Bollyky**[9], **Patrick Schrauwen**[8], **Hadi Al-Hasani**[5,6], **Michael Roden**[4,5,12], **Susanne Keipert**[5,13,14], **Antonio Vidal-Puig**[3,15], **Martin Jastroch**[5,13,14], **Judith Haendeler**[10,16], **Jens W. Fischer**[1]

[1]Institute of Pharmacology and Clinical Pharmacology, Medical Faculty, Heinrich-Heine-University Düsseldorf, Düsseldorf, Germany [2]Experimental Cardiovascular Imaging, Molecular Cardiology, Medical Faculty, Heinrich-Heine-University Düsseldorf, Düsseldorf, Germany [3]MRC Metabolic Diseases Unit, Metabolic Research Laboratories, University of Cambridge, Cambridge, United Kingdom [4]Institute for Clinical Diabetology, German Diabetes Center, Leibniz Center for Diabetes Research at the Heinrich-Heine-University Düsseldorf, Düsseldorf, Germany [5]German Center for Diabetes Research (DZD e.V.), München-Neuherberg, Germany [6]Institute for Clinical Biochemistry and Pathobiochemistry, Medical Faculty, German Diabetes Center, Leibniz Center for Diabetes Research at the Heinrich-Heine-University Düsseldorf, Düsseldorf, Germany [7]Human Genetics Program, Sanford Burnham Prebys Medical Discovery Institute, La Jolla, CA, USA [8]Department of Nutrition and Movement Sciences, Maastricht Medical Centre, NUTRIM School of Nutrition and Translational Research in Metabolism, The Netherlands [9]Division of Infectious Diseases and Geographic Medicine, Dept. of Medicine, Stanford University School of Medicine, Stanford, CA, USA [10]Institute for Clinical Chemistry, Medical Faculty, Heinrich-Heine-University Düsseldorf, Düsseldorf, Germany [11]Institute for Biomedical and Pharmaceutical Research, Nürnberg-Heroldsberg, Germany [12]Division of Endocrinology and Diabetology, Medical Faculty, Heinrich-Heine-University Düsseldorf, Düsseldorf, Germany [13]Institute for Diabetes and Obesity,

[*]**corresponding author**: Dr. Maria Grandoch, Institute of Pharmacology and Clinical Pharmacology, Medical Faculty, Heinrich-Heine-University Düsseldorf, Düsseldorf, Germany, maria.grandoch@hhu.de.

Reporting Summary. Further information on research design is available in the Nature Research Reporting Summary linked to this article.

Author Contributions

M.G. and J.W.F. developed the study, were involved in the design of all experimental protocols and wrote the manuscript. M.G., J.K.M., C.K., K.F and Y.O. were involved in data generation. U.F. performed MRI measurements; S.V. and T.V.-P. performed experiments for measuring maximum energy expenditure, food intake experiments, discussed the results and helped with the manuscript. T.J., C.G., J.H. and M.R. were involved in the measurements of mitochondrial respiration. T.R.C., Z.Z. and H.A.H. were involved in the calorimetric measurements at 4° C and the measurements of ex vivo glucose uptake. M.K. and F.S. performed mass spectrometry. E.B.M.N. and P.S. performed the experiments in human isolated brown adipocytes, analyzed and discussed the data. Y.Y. developed the ubiquitous *Has1*-deficient and inducible *Has2*-deficient mice. V.S., P.B., S.K., and M.J. discussed the results and helped with the manuscript. All authors contributed to the discussion of the results and writing of the manuscript.

Competing Financial Interests

No competing financial interests are reported by the authors.

Data Availability

Data that support the findings of this study are available from the corresponding author upon reasonable request.

Europe PMC Funders Author Manuscripts
Europe PMC Funders Author Manuscripts

Europe PMC Funders Author Manuscripts

Europe PMC Funders Author Manuscripts

Helmholtz Diabetes Center, Helmholtz Zentrum München [14]Department of Molecular Biosciences, The Wenner-Gren Institute, The Arrhenius Laboratories F3, Stockholm University, SE-106 91 Stockholm, Sweden [15]WT-MRC Institute of Metabolic Science, University of Cambridge, Cambridge, United Kingdom [16]IUF - Leibniz Research Institute for Environmental Medicine, Heisenberg Group - Environmentally-induced Cardiovascular Degeneration, Düsseldorf, Germany

Abstract

Therapeutic increase of brown adipose tissue (BAT) thermogenesis is of great interest as BAT activation counteracts obesity and insulin resistance. Hyaluronan (HA) is a glycosaminoglycan, found in the extracellular matrix, which is synthesized by HA synthases (Has1/Has2/Has3) from sugar precursors and accumulates in diabetic conditions. Its synthesis can be inhibited by the small molecule 4-methylumbelliferone (4-MU). Here, we show that the inhibition of HA-synthesis by 4-MU or genetic deletion of *Has2/Has3* improves BAT`s thermogenic capacity, reduces body weight gain, and improves glucose homeostasis independently from adrenergic stimulation in mice on diabetogenic diet, as shown by a magnetic resonance T2 mapping approach. Inhibition of HA synthesis increases glycolysis, BAT respiration and uncoupling protein 1 expression. In addition, we show that 4-MU increases BAT capacity without inducing chronic stimulation and propose that 4-MU, a clinically approved prescription-free drug, could be repurposed to treat obesity and diabetes.

Brown adipose tissue (BAT) contributes to metabolic homeostasis in both rodents and humans[1,2]. BAT`s main function is to maintain body temperature via non-shivering thermogenesis. In addition, BAT has a remarkable capacity for glucose and triglyceride uptake and secretes adipokines that positively influence metabolism[3–5]. BAT activation counteracts obesity and insulin resistance (IR) by elevating total energy expenditure, supporting weight loss, and increasing insulin sensitivity[6,7].

Thus, new therapeutic strategies are of great clinical interest because existing weight-lowering drugs lack sufficient efficacy and raise safety concerns when used long-term[8,9–11].

Although BAT activation is an attractive strategy for supporting weight loss, the unfavourable or not yet extensively studied risk/benefit ratios of currently-known BAT activators, such as beta-adrenergic sympathomimetics[12], peroxisome proliferator-activated receptor γ (PPARγ) agonists[13], and fibroblast growth factor (FGF) 21[14], have hampered their clinical use. A large proportion of particularly obese individuals do not have detectable BAT[15,16]. Thus, being able to recruit and to activate more BAT is important, urgently requiring new compounds that increase BAT activity. Relatedly, there is also a need for improving the technologies to measure BAT activity. To date, BAT activity is assessed *in vivo* using CT-guided ^{18}F-fluorodeoxyglucose positron emission tomography (^{18}F-PDG-PET)[2]. However, this method has its limitations, especially in states with increased insulin resistance. Developing new BAT activators would be fostered by effective non-radioactive imaging methods for longitudinal analysis of BAT activity *in vivo*.

Europe PMC Funders Author Manuscripts

Europe PMC Funders Author Manuscripts

Hyaluronan (HA), a long, non-sulfated glucosaminoglycan, is abundant in the extracellular matrix. The transmembrane HA synthases (HAS)-1, -2, and -3 catalyze HA synthesis from activated sugar precursors, namely uridine diphosphate (UDP)-glucuronic acid (UDP-GlcUA) and UDP-N-acetyl-glucosamine (UDP-GlcNAc), thereby linking HA synthesis to glucose metabolism[17]. Indeed, HA is strongly affected by diabetic conditions[18]. In turn, since glucose reportedly also serves as an important BAT substrate in cold-induced thermogenesis[19], changes in HA synthesis might directly impact BAT function. The small molecule inhibitor 4-methylumbelliferone (4-MU; INN “hymecromone”) has been used in humans as a prescription-free choleretic drug and is available in Europe and Asia.

It is also used as an inhibitor of HA biosynthesis by competing with the endogenous substrates for UDP-glucuronyltransferase, thereby depleting the cytosolic UDP-GlcUA pool[20]. In turn, the HA precursors GlcUA and GlcNAc accumulate and might be directed into other catabolic pathways or used for post-translational modifications such as *O*-GlcNAcylation.

Given the interference of HA with glucose metabolism, we hypothesized that HA synthesis interferes with BAT function. Therefore, the aims of the present study are to test the effect of the small molecule inhibitor of HA synthesis on BAT activity and to investigate the underlying mechanisms using HAS isoenzyme-deficient mice. Relatedly, to facilitate longitudinal analysis of BAT activity, we aimed to develop a novel MRI-based method for functionally assessing BAT activation.

Here, we demonstrate that inhibition of HA synthesis by 4-MU induces thermogenic markers in primary human brown adipocytes and in mice, increases BAT capacity while ameliorating hyperglycemia and the development of obesity. Further, we present a novel MRI T2 mapping method capable of assessing BAT function *in vivo*. Importantly, both 4-MU and the magnetic resonance imaging (MRI)-based BAT imaging have the potential to be directly translated into patients.

Results

4-MU prevents weight gain and activates BAT

8-week-old male C57Bl6/J mice were fed a diabetogenic diet (DD) supplemented with or without 4-MU (DD 4-MU). Plasma levels in mice reached values of 56.08 ± 0.009 ng/ml after 24 hours of 4-MU treatment, which resembles the concentrations achieved in humans treated with the compound. Importantly in the context of this manuscript, 4-MU accumulated in BAT reaching tissue concentrations of 6.16 ± 2.90 μg/mg.

4-MU treatment reduced weight gain and total body fat content, as determined by NMR analysis after 17 weeks of feeding (Figure 1a, b). In order to elucidate the underlying mechanisms leading to this dramatic phenotype, (i) food intake, (ii) hormonal factors, and (iii) spontaneous activity of the mice were analyzed. Food intake during chronic administration was not affected in DD 4-MU-treated mice compared to DD-fed mice thereby excluding an anorectic effect (Figure 1c). Also, within one week of pair-feeding, 4-MU decreased weight gain and BAT weight, thereby revealing that the effect of 4-MU did not

Europe PMC Funders Author Manuscripts

Europe PMC Funders Author Manuscripts

depend on food intake (Supplementary Figure 1). Circulating triglycerides and cholesterol levels were unchanged (Supplementary Figure 2) while circulating leptin was reduced in 4-MU treated animals (Figure 1d), thereby excluding involvement of changes in hepatic metabolism and central leptin-mediated behavioral and metabolic responses induced by 4-MU. Further, after 5 weeks of feeding, no increase in locomotor activity of 4-MU-treated mice was detectable (Supplementary Figure 3), despite significantly reduced weight of the animals as shown in Figure 1a.

Importantly, interscapular BAT weight was dramatically reduced, and BAT adipocytes were smaller in 4-MU treated mice; both indicating decreased lipid content (Figure 1e-h). 4-MU induced *Ucp1* and *Cidea* mRNA expression in BAT after 22 weeks of feeding (Figure 1i), pointing towards increased BAT capacity. Of note, increased expression of *Ucp1* mRNA in BAT was detected even at 6 and 9 hours after 4-MU treatment, well before changes in body weight occurred (Supplementary Figure 4). Consistent with this, immunohistochemical staining of BAT as well as western blots of UCP1 demonstrated elevated protein expression in 4-MU-treated mice (Figure 1j,k).

Importantly, elevated levels of UCP1 occurred independently from changes in sympathetic nerve density, as shown by western blot analysis of tyrosine hydroxylase expression in BAT of mice treated for 22 weeks with DD or DD 4-MU (Figure 1l). In addition, pretreatment of mice with the unselective β receptor antagonist propranolol prior to 4-MU application had no effect on 4-MU-induced changes in BAT weight and *Ucp1* mRNA expression (Supplementary Figure 5). Accordingly, 4-MU likewise increased the expression of *Ucp1*, *Cidea*, and *Ppargc1a* mRNA in differentiated murine primary brown adipocytes (Supplementary Figure 6a-c) as well as in murine T37i cells (Supplementary Figure 6d), and differentiated adipocytes derived from human BAT (Figure 1m and Supplementary Figure 6e). These *in vitro* results confirmed the cell-autonomous effects of 4-MU on *Ucp1* regulation and suggests potential translational relevance, since the effect was also observed in primary human brown adipocytes (although the number of patients has yet to be increased for statistical analysis).

Furthermore, we investigated 4-MU effects in thermoneutrality (30°C), where BAT thermogenesis is minimized. After one month of adaptation, mice received either only DD or DD supplemented with 4-MU for two weeks. Interestingly, 4-MU treatment reduced weight gain as observed before at 21°C (Supplementary Figure 7a). The identical effects were seen at 30°C in pair-fed groups (DD (30°C) 105.5% ± 2.75% weight gain versus DD 4-MU (30°C) 103.9% ± 3.69% weight gain, mean ± s.e.m.). Likewise, 4-MU reduced BAT weight, decreased adipocyte size (Supplementary Figure 7b,c), and increased *Ucp1* expression in BAT while *Cidea* and *Ppargc1a* mRNA expression were not affected (Supplementary Figure 7d-f) at 30°C.

Next, we investigated whether 4-MU`s effects were restricted to BAT or whether effects also occur in WAT. Indeed, beiging of inguinal adipose tissue (AT) was observed in 4-MU-treated animals, as seen in the gene expression of previously described beige adipocyte markers[21] *Ucp1*, *Ppargc1a, Tnfrsf9*, *Tbx1*, and *Tmem26* was upregulated (Supplementary Figure 8a-e).

Europe PMC Funders Author Manuscripts

Europe PMC Funders Author Manuscripts

The presence of multilocular, UCP1-positive adipocytes in 4-MU-treated mice was further confirmed by immunohistological staining of inguinal AT (Supplementary Figure 8f, g).

4-MU improves glucose tolerance and insulin resistance

In line with 4-MU`s strong effects on body weight gain and BAT activation, glucose homeostasis was beneficially affected, and insulin sensitivity was improved in 4-MU-treated mice (Figure 2a,b). Further, plasma insulin was decreased in fasted mice (Figure 2c). Thus, 4-MU treatment prevents the weight gain and the development of insulin resistance (IR) that is normally observed in mice on DD.

4-MU reduces white AT hypertrophy and inflammation

Since different types of AT (white, brown, beige) in concert regulate energy balance and metabolic homeostasis, we examined 4-MU effects on WAT in more detail. Analyzing the epididymal AT revealed a strong effect of 4-MU: we detected reduced fat pad weight and decreased adipocyte size, paralleled with reduced numbers of AT macrophages and decreased mRNA expression of pro-inflammatory cytokines such as *Ccl2* and *Il1β* (Supplementary Figure 9a-e). In accordance with these results and supporting 4-MU's beneficial effect on energy and glucose homeostasis, insulin-stimulated glucose uptake increased in freshly isolated adipose cells from 4-MU-treated mice (Supplementary Figure 9f).

4-MU halts obesity and reverses IR

In order to evaluate the therapeutic potential of 4-MU treatment, mice were first fed with DD for 8 weeks in order to develop obesity and IR. Animals were then randomized to two groups equivalent in body weight and fasting blood glucose (Supplementary Figure 10a,b). Then the groups were fed either DD alone or DD 4-MU for additional two weeks. As shown in Supplementary Figure 10c, 4-MU prevented further weight gain and reduced fasting blood glucose while glucose tolerance was slightly affected (Supplementary Figure 10d,e). These results underline 4-MU's beneficial effects even on already established obesity and IR.

4-MU increases BAT`s thermogenic capacity

Collectively, the results strongly suggest increased BAT capacity in 4-MU treated mice. Next, energy expenditure at room temperature and at 4°C was analyzed in detail. Surprisingly, although UCP1 was significantly upregulated on mRNA and protein levels (Figure 1i,j), experiments at 21°C room temperature indicated that 4-MU-treated mice display reduced metabolic rates (Figure 3a). However, when challenged by cold exposure (switching them to 4°C), mice on DD 4-MU diet increased their metabolic rate by greater extent than controls (Figure 3b,d). In this way, differences in energy expenditure observed at 21°C were abolished after cold exposure (Figure 3c,d). These results pointed towards a higher thermogenic capacity of BAT after treatment with 4-MU, which was further confirmed by measuring the maximum energy expenditure of 4-MU-treated and control mice following stimulation with norepinephrine (NE). When corrected for body weight by using ANCOVA, the maximum NE-stimulated energy expenditure in 4-MU-treated mice

Europe PMC Funders Author Manuscripts

Europe PMC Funders Author Manuscripts

was greater than in controls (Figure 3e-g), suggesting they had a disproportionately increased thermogenic capacity. In line and in support of these hypotheses of increased thermogenic capacity in 4-MU treated mice, the UCP1 protein content per gram of BAT was increased despite the lower total BAT weight, in both mice cohorts, after long-term-treatment for 22 weeks (Figure 3h) and after acute 24- hour 4-MU application (Figure 3i).

MRI of increased BAT capacity

Because 4-MU reduced weight gain rapidly within the first week of feeding (Figure 1), including under pair-feeding conditions (Supplementary Figure 1), we analyzed the underlying mechanisms of short-term treatment. To monitor the acute impact of 4-MU on BAT function, we validated a novel MRI approach for non-invasively visualizing BAT activity.

For this, we harnessed the susceptibility of the MRI relaxation time T2 to regional magnetic field inhomogeneities. Due to its heterogeneous tissue composition, high iron content, and rich vasculature, BAT's baseline T2 values are substantially lower than in WAT (Figure 4a,c; Supplementary Figure 11,12). We expected this effect would be even more pronounced under BAT activation, resulting in higher metabolic turnover, heat production, and perfusion. To test this assumption, mice were subjected to T2 mapping immediately before and 1 hour after pharmacological β3-adrenergic stimulation (CL-316,243). Application of the β3 agonist resulted in substantially decreased T2 in dorsocervical BAT, as represented by a shift from yellow to red in the color-coded maps (Figure 4a). Quantification of the entire BAT area (Figure 4b and Supplementary Movie) revealed significantly lower T2 values after β3-adrenergic stimulation. Importantly, this T2 reduction was restricted to BAT segments: neither skeletal muscle nor WAT T2 was significantly altered by CL-316,243 (Figure 4c). The T2 sensitivity for BAT activation was corroborated in mice challenged by cold exposure: After 2.5 h at 4 °C, BAT T2 dropped to a similar magnitude as observed for CL-316,243 (Figure 4d and Supplementary Figure 12a). Further, we compared BAT volume as detected by MRI with the BAT weight after harvesting interscapular BAT tissue, revealing a strong correlation between the BAT mass predicted by MRI and based on biopsy (Supplementary Figure 12e,f)

After confirming the specificity and sensitivity of this approach for BAT activation, mice treated for 24 h with 4-MU were examined by T2 mapping. Supplementary Figure 15c shows that 4-MU treatment results in a drop of T2 confirming BAT activation. Quantification revealed that BAT T2 decreased to approximately 60% of the effect found for β3-adrenergic stimulation and cold exposure (Figure 4d). Planimetry of the BAT segments, including all interscapular and dorsocervical depots (Figure 4b, Supplementary Movie), showed that 4-MU treatment for 24 h substantially reduced total BAT volume (Figure 4e), thereby indicating enhanced lipolysis.

Also using this novel MRI approach, activation of the SNS could be excluded using 4-MU in combination with a β3-specific antagonist, L-748,337. While L-748,337 inhibited the CL-316,243-mediated increase of *Ucp1* mRNA expression (CL-316,243: 2.473 ± 0.603 fold increase versus control; L-748,337 + CL-316,243: 0.124 ± 0.02; mean ± s.e.m.), treating mice with 4-MU for 24 h in the presence of L-748,337 demonstrated that 4-MU acutely

Europe PMC Funders Author Manuscripts

Europe PMC Funders Author Manuscripts

activates BAT independently of β-adrenergic stimulation (Figure 4d). These results strongly underline that 4-MU's long-term and short-term effects on BAT are direct and do not depend on sympathetic stimulation.

4-MU enhances mitochondrial function

Given the impact of 4-MU on NE-stimulated energy expenditure, we investigated whether 4-MU increases mitochondrial function and cellular respiration. For this purpose, BAT mitochondria were isolated after 24 hours of 4-MU treatment, and increased state 3 respiration with complex I substrates was detected in isolated BAT mitochondria (Figure 4h). In line with this result, increased amounts of complex I were found by western blot in BAT from 4-MU treated mice (Supplementary Figure 13a). In contrast, no effects were detectable in isolated mitochondria from inguinal AT (Figure 4j). In both AT depots, citrate synthase activity (CSA), a marker of mitochondrial density, was not significantly altered (Figure 4i,k). 4-MU activation of BAT respiration was also detected in lysed BAT tissue by measuring O_2 flux after 22 weeks of feeding (Supplementary Figure 13b). Specifically, also in these tissue lysates, complex I-linked respiration increased in BAT isolated from 4-MU-treated mice while CSA was not significantly different between the treatment groups (Supplementary Figure 13c). Thus, both short-term (Figure 4h, i) and long-term exposure (Supplementary Figure 13b,c) to 4-MU increased respiration in BAT.

4-MU increases glycolysis and vascularization in BAT

Next, the underlying mechanisms leading to enhanced BAT activation were investigated. Since HA synthesis is dependent on activated sugar precursors, we considered that inhibition of HA synthesis will interfere with the glucose metabolism. Indeed, *Slc2a4* mRNA expression and multiple glycolytic enzymes were increased in BAT of animals treated with 4-MU for 24 hours (Figure 5a-f). In line, elevated glucose and lactate levels were found in BAT after acute treatment with the compound (Figure 5g). To corroborate that 4-MU-mediated effects depend on glycolysis, we used the glucose derivate 2-deoxy-D-glucose (2-DG). 2-DG is metabolized into 2-DG-phosphate, which cannot be further metabolized, resulting in the inhibition of glycolysis. Co-treating mice with 2-DG and 4-MU completely abolished 4-MU-induced *Ucp*1-mRNA expression (4-MU: 3.62 ± 0.83 fold increase versus control; 2-DG+ 4-MU: 0.41 ± 0.07 fold increase versus control; mean ± s.e.m.) as well as the decrease in BAT weight/body weight ratio. Importantly, the glycolytic end product lactate, which is also increased in T37i brown preadipocytes treated with 4-MU, has been previously described as a browning agent in subcutaneous adipose tissue. In this study, lactate stimulated *Ucp1* expression in T37i brown preadipocytes after 24 hours in a dose-dependent way (Figure 5h,i).

Further evidence for changes in substrate usage of 4-MU treated mice is seen in the respiratory exchange ratio (RER): while the RER in 4-MU-treated mice was reduced at 21°C (indicating greater lipid oxidation), increased RER during cold exposure (compared to the DD-fed control group) indicates enhanced carbohydrate oxidation (Supplementary Figure 12a). In line with this observation, lipolysis was increased in BAT of 4-MU fed mice at 21°C as detected by induction of hormone-sensitive lipase RNA and protein (Supplementary

Europe PMC Funders Author Manuscripts

Europe PMC Funders Author Manuscripts

Figure 12a,b). Furthermore, plasma levels of non-esterified fatty acids were increased (Supplementary Figure 12c).

As a proof of concept showing that UCP1 upregulation is responsible for the metabolic phenotype of 4-MU-treated mice, *Ucp1*-deficient mice were fed either DD or DD plus 4-MU. No effects of 4-MU were observed in *Ucp1*-deficient mice with respect to body weight gain, glucose homeostasis as well as BAT T2 relaxation time and tissue weights of BAT and liver (Supplementary Figure 15).

In addition to the mechanisms described above, glycolysis is also known to promote angiogenesis, another crucial process for BAT activation. Indeed, *Vegfa* mRNA expression was strongly augmented, and isolectin staining confirmed higher BAT vascularization after chronic 4-MU treatment for 22 weeks (Figure 5j-l).

Has2/3 DKO mice mimic 4-MU`s beneficial metabolic phenotype

Finally, we asked whether inhibition of HA synthesis is indeed responsible for the increase of BAT`s thermogenic capacity by 4-MU. First, we analyzed HA-synthesizing enzyme expression: *Has2* and *-3* were the most abundant HA synthase isoenzymes in BAT (Supplementary Figure 16a). Of note, after cold exposure for 8 hours, known to acutely stimulate BAT activity, a strong downregulation of all HAS isoenzymes was observed (Supplementary Figure 16b). This may be the physiological equivalent to the herein postulated interrelationship between BAT activity and HA synthesis.

Analyzing mouse strains with only a single HA synthase isoenzyme knockout revealed no major changes in the metabolic phenotype (Supplementary Figure 17 - 19).

However, mice with genetic deficiency in the two most abundant HAS isoenzymes, *Has2/3* DKO, exhibited significantly less weight gain on DD (Figure 6a), similar to the effects of 4-MU treatment. In line with this, body fat content declined (Figure 6b). However, glucose tolerance tests showed no significant effect of *Has2/3* DKO (Figure 6c). We also observed lower BAT volume, BAT weight and a significantly decreased T2 time in BAT from *Has2/3* DKO versus respective control animals. In contrast, T2 of WAT and muscle were not altered between the genotypes, thereby underlining the BAT-specific effects of *Has2/3* deficiency (Figure 6d-g). The mRNA expression of *Ucp1* was increased, together with trends in elevated *Cidea* and *Ppargc1a* mRNA (Figure 6h). In inguinal AT, *Ppargc1a* and *Tmem26* m*R*NA expression were increased while other beiging markers showed no changes (Supplementary Figure 20). However, energy expenditure was not significantly altered in *Has2/3* DKO (Figure 6i) compared to WT controls. The RER was slightly shifted towards carbohydrate consumption (Figure 6j).

Together, these results suggest that inhibition of HA synthesis shifts the metabolic flux towards glycolysis, possibly supporting mitochondrial respiration. Additional effects of FA (derived from *de novo* lipogenesis) and lactate further promote these effects. Genetic deficiency of *Has2 and -3* largely mimicks the effects of the pharmacological inhibitor of HA synthesis, 4-MU, although not in all aspects. A summarizing scheme of 4-MU`s postulated mechanisms of action is provided in Figure 7.

Europe PMC Funders Author Manuscripts

Europe PMC Funders Author Manuscripts

Discussion

Developing agents that safely and effectively activate BAT is an exciting frontier in obesity and diabetes research. In the last years, the development of compounds activating BAT as a novel therapeutic option has been fostered for treating obesity and T2DM. Indeed, BAT activation has been shown to effectively reduce blood glucose in diabetic patients[7,22].

Two options are currently favoured when trying to increase BAT thermogenesis: either increasing the amount of BAT or increasing BAT activity. However, the therapeutic success of increasing the amount of BAT depends upon ensuring simultaneous activation by respective mechanisms which might lead to concomitant unfavourable systemic responses. Indeed, strategies trying to target BAT function pharmacologically can have serious side effects, especially due to parallel SNS activation.

Here we show that inhibiting HA synthesis increases BAT`s thermogenic capacity. Deletion of a single HA synthase was not sufficient to impose any effects on systemic metabolism. However, if the two most abundant HAS isoenzymes in BAT, namely HAS2 and HAS3, were deleted, a reduction in total amounts of HA were achieved and the beneficial metabolic effects of 4-MU were mimicked, thereby uncovering the interrelationship of BAT thermogenic capacity and HA synthesis.

Importantly, 4-MU-induced effects were independent of sympathetic activation, thereby being of major relevance to the compound’s potential use in humans. This was shown by using a β3-specific antagonist (L-478,337) as well as the unselective β receptor antagonist propranolol: both substances did not prevent the 4-MU-induced increase in *Ucp1* mRNA expression while *Ucp1* upregulation by the beta3 receptor -specific agonist was effectively blunted by both β receptor antagonists. In line, 4-MU effects were also seen at thermoneutrality and 4-MU also increased *Ucp1* mRNA expression *in vitro* by cell-autonomous mechanisms. The potential effectiveness in humans is underlined by 4-MU effects on *Ucp1* mRNA expression in primary human brown adipocytes, although the limited number of patients included here has to be taken into account as a limitation.

In our study, 4-MU attenuated body weight gain, improved glucose homeostasis and BAT`s thermogenic capacity in mice. We did not observe any changes in food intake during chronic treatment, and also demonstrated reduced body weight gain in pair-fed mice, in mice receiving 4-MU independently by oral gavage and in *Has2/3* DKOs and wildtype mice. In addition, effects on BAT and increased *Ucp1* mRNA expression were already detected as early as 6-9 hours after 4-MU treatment before changes in body weight. In sum, all of these points suggest that 4-MU’s beneficial long-term metabolic effects are mediated directly by the compound`s inhibition of HA synthesis.

Mechanistically, it was found that BAT`s maximum thermogenic capacity was increased when challenged by cold exposure or NE. This was further confirmed by the finding of an increased total UCP1 amount per BAT depot in 4-MU treated mice. The causal role of UCP1 was demonstrated in *Ucp1*–deficient mice, where 4-MU showed no metabolic effects as observed before in C57BL/6 wildtype mice.

Europe PMC Funders Author Manuscripts

Europe PMC Funders Author Manuscripts

Consistent with its effects on maximum NE-stimulated energy expenditure, 4-MU increased BAT respiration and specifically increased the activity of mitochondrial complex I, shown in both, BAT and isolated BAT mitochondria derived from 4-MU-treated mice. Complex I activity is directly linked to increased respiratory chain activity and UCP1-mediated thermogenesis in BAT[23].

In searching for the upstream mechanism that leads to increased BAT respiration, we considered enhanced substrate flow into the glycolytic pathway. Glucose is an important substrate for BAT thermogenesis, especially during cold exposure, thereby also regulating systemic glucose homeostasis and increasing energy expenditure[4,19,22]. HA synthesis consumes activated UDP-sugars[24] and inhibiting HA synthesis might increase the glycolytic pathway thereby providing more substrates for mitochondrial respiration. In line, the glycolysis inhibitor 2-DG abolished 4-MU-induced increase in BAT activity and RER was increased by 4-MU at 4°C indicating more carbohydrate consumption under conditions of acute stimulation. Furthermore, and in support of increased glucose utilization, 4-MU increased *Slc2a4* mRNA expression.

We also detected elevated lactate levels – corresponding to enhanced glycolysis – in response to 4-MU *ex vivo and in vitro*. Indeed, lactate itself has been proposed as a browning agent in subcutaneous AT[25]. In murine brown preadipocytes, lactate directly upregulated *Ucp1* expression *in vitro* pointing towards direct effects. Of note, a recent paper also reported on the relevance of circulating lactate as an important TCA substrate[26] which might also drive the increased flux to the respiratory chain. Further, since glucose is not the primary substrate for thermogenesis, *de novo* lipogenesis (DNL) and subsequent fatty acid oxidation likely also contribute as previously described[27,28] in 4-MU treated mice.

Of note, activating effects of 4-MU were mainly observed in BAT while the beiging effects on inguinal AT were much less pronounced or even missing such as the effect on complex I activation. This might be due to the fact that beige adipocytes are dispersed within the subcutaneous AT depot so that the mixture of cells may have masked the 4-MU effect seen in pure brown adipocytes or even side-specific actions of 4-MU in BAT. This will be addressed in further studies. Therefore, we think that beiging might contribute to the overall 4-MU induced phenotype but to a lesser extent than BAT.

In addition to its acute effects, 4-MU also induced long-term effects that could support improved BAT activity. We detected enhanced *Vegfa* expression and augmented BAT vascularization after 22 weeks of 4-MU treatment. Interestingly, angiogenesis has also been reported to contribute to BAT activation and depend strongly on glycolysis[10,29,30]. The aforementioned increase in glycolytic substrates might therefore also contribute to BAT vascularization in the presence of 4-MU. In addition, a recent study also described the autocrine effects of VEGF-A on mitochondrial function and thermogenesis; these effects might contribute to the observed phenotype[23]. Furthermore, and in line with previous reports, we detected reduced WAT mass and WAT inflammation following 4-MU treatment. These reductions likely contribute to the systemically-improved metabolic phenotype in chronically treated mice[31,32].

Europe PMC Funders Author Manuscripts

Europe PMC Funders Author Manuscripts

Characterizing 4-MU's effect on BAT *in vivo* was facilitated by the present T2 mapping approach. The current gold standard for functional BAT imaging is CT-guided ^{18}F-FDG-PET[2]. Recent MRI studies mainly focused on the relaxation parameter T2* to assess the metabolic activity of BAT[33,34]. However, alterations in T2* are balanced by two opposing effects under BAT activation: while deoxyhemoglobin, produced by oxidative metabolism, reduces T2*, the enhanced blood flow increases T2*. Compared to T2*, T2 mapping is less prone to susceptibility artifacts especially at high magnetic fields and, thus, seems to be more robust for monitoring BAT activation. Validated by both pharmacological and physiological stimulation, this method facilitated the characterization of 4-MU in this study. Further, T2 mapping has the potential to assess BAT activity in humans without any harmful contrast agent or radiation and could also facilitate the development of new BAT activators.

In summary, we describe here 4-MU as a new small molecule inhibitor increasing BAT activatibility and promoting its thermogenic capacity by inhibition of HA synthesis which causes redirection of substrates into the glycolytic pathway. This increases DNL thereby providing substrate for lipolysis and beta oxidation as well as also increasing levels of lactate/pyruvate which in turn serve as substrates for mitochondrial complex I respiration and increase UCP1 expression (Figure 7). At later stages, other factors, such as increased BAT vascularization and decreased WAT inflammation, might contribute to the overall protective effects against the development of obesity and IR.

Limitations of the current study include the lack of more extensive human data including in vitro experiments in isolated brown preadipocytes as well as a first translation of the novel T2 mapping approach in humans. These will be addressed in more detail in the future. In this context it is yet unclear how much of the beneficial effects seen in mice might also translate to humans where the amount of BAT is highly variable between different subjects and different comorbidities.

Despite these limitations the present study clearly underlines the importance of BAT for whole body metabolism and the opportunity to prevent obesity as well as T2DM with BAT-focussed approaches. For the first time a regulatory role of the HA-rich ECM is shown in regulating BAT activity by changing intracellular substrate fluxes. Therefore, HA might be a valuable novel target in the attempt to improve BAT activity which might be even preferable compared to therapeutic approaches solely focusing on increasing BAT mass.

Of note, inhibiting HA synthesis by either 4-MU treatment or by genetically deleting HAS isoenzymes improves BAT capacity independently from sympathetic stimuli. Thus, unfavorable side-effects as reported for many other recently described BAT activators can be excluded. In line, also chronic BAT stimulation which in turn might also have harmful effects on systemic metabolism was avoided. Both, the T2 mapping protocol and the use of 4-MU to pharmacologically activate BAT, have clear translational utility because 4-MU has been used for many years in clinical practice[35,36,37].

Europe PMC Funders Author Manuscripts

Europe PMC Funders Author Manuscripts

Methods

Animal studies

All animal experiments were conducted according to the guidelines for the use of experimental animals as given by “Deutsches Tierschutzgesetz” and approved by the local Research Board for animal experimentation (Landesamt für Natur, Umwelt und Verbraucherschutz NRW; State Agency for Nature, Environment and Consumer Protection). All experiments were conducted in at least three independent groups of mice with free access to water and food (except for pair-feeding experiments) and were conducted at 22° C ± 1° C ambient temperature (except for experiments under thermoneutral conditions) and a 12 h day-night cycle. Investigators were not blinded to the group allocation or the genotype of the mice. Blinded data collection and/or analysis were performed in following experiments: histological stainings, qPCR, MRI measurements *in vivo* and *ex vivo*, ELISA and fluorometric assays, western blot analysis, the CSA/BAT and the oxygraph measurements.

Mouse strains

For all experiments only male mice were used. Female mice were not used due to major differences in the development of obesity and insulin-resistance. Littermate controls were used for experiments. Pre-established exclusion criteria were defined stating that all mice with an insufficient knock down of the target genes by tamoxifen-treatment (> 70%) were excluded from the experiments. Further, mice were excluded from the experiment when certain criteria of suffering were observed. These included weight loss greater than 20 % of body weight, cessation of food and water ingestion or lack of voluntary movement.

C57BL/6J wild-type mice were obtained from Janvier Labs (Le Genest-Saint-Isle, France) or from an in-house breeding of the same strain. For determination of maximum energy expenditure C57BL/6 were purchased from Charles River UK. This research has been regulated under the Animals (Scientific Procedures) Act 1986 Amendment Regulations 2012 following ethical review by the University of Cambridge Animal Welfare and Ethical Review Body (AWERB). Animals were housed in a specific pathogen free facility with 12 hour light and 12 hour dark cycles.

Ucp1-deficient mice (B6.129-Ucp1tm1Kz/J; on C57BL/6J background – originally from Jackson Laboratory) were kindly provided by Martin Jastroch (Helmholtz-Zentrum München, Germany). Mice were bred, born and weaned at 30°C. All subsequent analyses were performed at 30°C.

Ubiquitous *Has1*-deficient mice (C57BL/6J.Cg-Has1^{tm})[38] and *Has2*$^{flox/flox}$ mice, kindly provided by Yu Yamaguchi[39], were all on C57BL/6J background. Rosa26CreER$^{T2+/-}$ mice (Taconic; Hudson, NY, USA)[40] were crossed with *Has2*$^{flox/flox}$ mice[39] to generate ubiquitous conditional *Has2*-deficient mice (Rosa26CreER$^{T2+/-}$;*Has2*$^{flox/flox}$), on C57BL/6J background.

Mice floxed for *HAS3 (HAS3KI*$^{flox/flox}$) were generated by GenOway (Lyon, France) and used for generation of ubiquitous constitutive *Has3*-deficient (*Has3* KO) mice, both

Europe PMC Funders Author Manuscripts

Europe PMC Funders Author Manuscripts

backcrossed on C57BL/6J background. Generation of these mice is described in detail in Kiene *et. al*, 2016.[41]

Ubiquitous *Has2/Has3* double-deficient (*Has2/3*-DKO) mice were generated by crossing the Rosa26CreER$^{T2+/-}$;*Has2*$^{flox/flox}$ mice with ubiquitous *Has3*-KO) mice.

Feeding

Starting at the age of 8 – 10 weeks, age-matched C57BL/6J mice were randomly assigned to two treatment groups receiving either standard diabetogenic diet (DD; composed of 59 % kcal derived from fat and 26 % kcal derived from carbohydrates; ssniff, Soest, Germany) supplemented with either 50 g/kg 4-methylumbelliferone (4-MU; Sigma Aldrich, St. Louis, MO, USA) or DD with respective placebo for up to 22 weeks.

Feeding experiments of *Has1,-2 or -3* single-deficient, *Has2/Has3* double-deficient and *Ucp1*-deficient mice started at 16-20 weeks. For induction of the *Has2*-knockout, 16 – 20 weeks old Rosa26CreER$^{T2+/-}$;Has2$^{flox/flox}$, Rosa26CreER$^{T2+/-}$;*Has2*$^{flox/flox}$/*Has3*$^{-/-}$ and respective Rosa26CreER$^{T2+/-}$ control mice were treated daily with 4 mg tamoxifen (Sigma Aldrich, St. Louis, MO, USA) by oral gavage for 5 days. One week after the last tamoxifen treatment mice were fed with DD up to 22 weeks. Afterwards, mice were sacrificed and tissues were taken for further analysis.

Food intake was analyzed during the first 11 weeks of feeding by weighing the food that was consumed within one week.

For pair-feeding experiments, C57BL/6J mice in the DD control group received the same amount of diet per day as consumed by the DD 4-MU-treated mice at start of the experiment at 8-10 weeks of age. Body weight was recorded every second day for one week.

For studying the acute effects of 4-MU treatment, mice received 4-MU or respective placebo via oral gavage (300 mg/mouse/day) for the indicated period of time.

For the experiments under thermoneutral conditions, 16 week old C57BL6/J mice were housed for 4 weeks at 30° C in a constant climate chamber (HPP770life, Memmert, Schwabach, Germany) before starting feeding DD or DD supplemented with 4-MU for additional two weeks.

NMR analysis of whole body composition

Total body fat content of mice was determined with a nuclear magnetic resonance (NMR) Analyzer Minispec and Minispec plus software (both Bruker Corporation, Billerica, MA, USA) after 11 or 17 weeks of feeding. Intraperitoneal glucose tolerance (ipGTT) and insulin tolerance tests (ITT) were performed after 13 or 19 and 14 or 20 weeks of feeding, respectively. After undergoing starvation for 6 hours, mice were injected with 1 g/kg BW glucose or 0.75 U/kg BW insulin. Blood glucose concentration was assessed before (fasting blood glucose) and (5,) 15, 30, 60 and 120 minutes post injection of glucose or insulin bolus.

For determination of therapeutic effects of 4-MU treatment on established glucose intolerance and obesity, 8-10-week-old C57BL/6J mice were fed with DD for 8 weeks.

Europe PMC Funders Author Manuscripts

Europe PMC Funders Author Manuscripts

Subsequently mice were randomly assigned to two groups which did not differ with regard to fasting blood glucose and body weight and treated for two weeks with DD or DD-4MU.

Metabolic measurements

Basal and cold-induced energy expenditure (Volume O_2) and the corresponding respiratory exchange ratios (RER) were assessed with a customized indirect calorimetry system (TSE PhenoMaster) and TSE PhenoMaster Software (both TSE Systems GmbH, Bad Homburg, Germany). For analysis of basal energy expenditure, C57BL/6J (fed with DD or DD 4MU for 11 weeks), *Has1,-2,-3* single-deficient, *Has2/-3* double-deficient mice and their respective control mice (fed with DD for 11 weeks) were allowed to adapt to their new environment for 72 hours, after which measurements were performed for additional 72 hours. For analysis of cold-induced energy expenditure, mice were allowed to adapt for 24 hours and were then exposed to cold (4° C) for additional 8 hours. All variables were assessed every 30 minutes during measurement.

Metabolic rate was calculated from energy expenditure by correcting for body weight using ANCOVA with body weight as a covariate, diet or genotype as a fixed factor and energy expenditure as the dependent variable. All analyses were performed using the general linear modelling function of SPSS 25.

Calorimetric measurements were performed at the following sites: the animal facilities at the HHU Düsseldorf, the German Diabetes Center Düsseldorf, Germany.as well as the Disease Model Core (MRC Metabolic Diseases Unit [MRC_MC_UU_12012/5], Cambridge, United Kingdom.

Thermogenic capacity measurement

8-10 week old C57BL/6 mice were fed DD 4-MU or DD control diet for 28 days as described before. To measure thermogenic capacity, mice were anaesthetised with 90 mg/kg pentobarbital and placed in a 2.7 l calorimetry chamber with a flow rate of 400 ml/min which was maintained at a temperature of 30°C. Room and chamber CO2% and O2% were measured every 4 minutes. Energy expenditure was calculated from VCO2 and VO2 using a modified Weir equation

Basal energy expenditure was measured until three stable readings were observed, which took ~24 minutes. Mice were then injected subcutaneously with 1mg/kg norepinephrine bistartrate and a further 30 mg/kg of pentobarbital. Energy expenditure was measured for a further 28 minutes until it plateaued.

The maximal NE-stimulated energy expenditure was determined as the average of the three largest readings post injection. The maximal NE-stimulated EE was highly correlated with body weight (P=0.001) and we corrected NE stimulated energy for body weight using ANCOVA with body weight as a covariate, diet as a fixed factor and NE-stimulated EE as the dependent variable. It was noted that one control animal exhibited a NE-stimulated EE that had a residual in the regression model that was 2.95 SD from the mean and was excluded from the analysis. All analyses were performed using the GLM function of SPSS.

Europe PMC Funders Author Manuscripts

Europe PMC Funders Author Manuscripts

Magnetic resonance imaging (MRI)

General setup—MRI data were recorded at a vertical Bruker AVANCE^{III} 9.4 T wide bore NMR spectrometer (Bruker, Rheinstetten, Germany) operated by ParaVision 5.1. Images were acquired using the Bruker microimaging unit Micro2.5 with actively shielded gradient sets (1.5 T/m) and a 25-mm birdcage resonator. Mice were anesthetized with 1.5 % isoflurane in a water-saturated gas mixture of 20 % oxygen in nitrogen applied at a rate of 75 ml/min by manually restraining the animal and placing its head in an in-house-built nose cone. Respiration was monitored by means of a pneumatic pillow positioned at the animal's back. Vital function was acquired by a M1025 system (SA Instruments, Stony Brook, NY, USA) and used to synchronize data acquisition with respiratory motion. Throughout the experiments mice were breathing spontaneously at a rate of approximately 100 min^{-1} and were kept at 37 °C. Animals were placed within the resonator that the field of view (FOV) in z-direction (~25 mm) covered a region from just below the cerebrum down to the heart.

Fat imaging—The localization of the brown adipose tissue (BAT) was determined by acquisition of images from the neck region using 2D ^{1}H multi-slice turbo spin echo (TSE) sequences with and without fat suppression. Data were taken from a FOV of 25.6×25.6 mm^2 with a matrix size (MS) of 256×192 resulting in a spatial resolution of 100×100 μm^2 after zero filling (TSE factor, 8; echo time (TE), 4.4 ms; repetition time (TR), 3500 ms; slices, 16; slice thickness (ST), 1 mm; acquisition time (TAcq), 84 s. Using the same receiver gain, two image sets were recorded with and without chemical shift selective fat suppression.

T2 mapping—Acquisition of T2 maps was carried out using a respiratory gated multi-slice multi-echo (MSME) sequence covering the entire BAT (8 slices, 16 echos, separated by a ΔTE of 3.805 ms; TR = 525 ms, ST = 1 mm, FOV = 25.6×25.6 mm^2, MS = 256×256 after zero filling, averages = 4, TAcq ≈ 5 min). Only one early trigger per expiration phase was used to provide constant conditions for the recording of the echo train. In order to create the T2 maps, an exponential decay curve was fitted to the intensity decline of each pixel within the 16 echo images using the image sequence analysis (ISA) tool of ParaVision (Supplemental Figure 9). For color coding of calculated T2 maps, a slightly modified version of the default color look-up table of ParaVision was applied. Demarcations for white and brown adipose tissue as well as muscle were manually drawn with the ParaVision Region-of-Interest (ROI) tool and tissue-specific T2 times were calculated from the respective ROIs (see supplemental Figure 9). For each of the 8 slices, 2 separated ROIs were evaluated for white adipose tissue (WAT) and muscle, respectively, while for BAT as many ROIs were used as required for entire coverage of all tissue parts (cf. supplemental Figure 9). From the area of these ROIs (multiplied with the slice thickness), the total BAT volume was calculated. To obtain tissue-specific T2 values for BAT, WAT, and muscle, data were averaged over the respective ROIs from all slices. For analysis of inguinal fat depots, the slice package was placed in axial orientation at the level of the hips and acquisition/ calculation of T2 maps was carried out as described above.

3D projections—For the 3D visualization of WAT and BAT in the upper part of the body, MR data were acquired with a 3D TSE sequence from the cerebrum down to the heart (TE = 3.5 ms; TR = 2500 ms, FOV = 25.6×25.6×25.6 mm^2, MS = 256×256×128 after zero filling,

Europe PMC Funders Author Manuscripts

Europe PMC Funders Author Manuscripts

resulting in a voxel size of 0.1×0.1×0.2 mm^3, averages = 3, TAcq = 32 min). Reconstructed image stacks were imported for further processing into the 3D visualization software Amira version 4.0 (FEI Visualization Sciences Group, Burlington, USA). MR signals were associated to the respective anatomical structures (BAT, WAT, spinal cord, brain, heart, and surrounding tissue) using the Segmentation Editor of Amira. For segmented areas, individual surfaces were calculated with unconstrained smoothing. Subsequently, semi-transparent surface views with “fancy alpha” were generated. Fade-out of the projections and concomitant rotation of the surface views were coordinated with the DemoMaker of Amira.

Analysis of substrate selection—Determination of tissue metabolite concentrations was essentially carried out by high-resolution MR spectroscopy using a 5-mm ^1H probe as previously described[42]. Blood-free tissues were rapidly excised, snap-frozen, and subsequently extracted with 1 mM perchloric acid (PCA). The extracts were neutralized, lyophilized, and stored at 20°C. Lyophilized PCA extracts were redissolved in 0.6 ml D2O and transferred into a 5-mm NMR tube. The pool size of various metabolites was quantified from fully relaxed high-resolution ^1H MR spectra. Trimethylsilyl-propionic-2,2,3,3d4-acid (TSP, 1 mM) was used to standardize the concentrations, and the results were correlated with the protein content of the samples.

BAT stimulation—All C57BL/J6 mice served as their own control, in that they were subjected to MRI measurements at baseline and after exposure to the adrenergic β3 agonist CL-316,243 solution (CL-316; 1 mg/kg; Tocris Bioscience, Bristol, UK), cold, and 4-MU respectively. This might implicate a certain limitation with regard to the accurate relocation of the MR slices for spatial correlation before and after BAT activation. However, at both time points all datasets were recorded over the entire BAT area, so that this does not introduce a bias into the comparison of the different stimuli. After the baseline MRI measurements, mice either (i) received for pharmacological β3 adrenergic activation an intraperitoneal bolus injection of CL-316[43] and were reintroduced into the scanner after 1 h, (ii) were exposed for 2.5 h to 4 °C and thereafter immediately subjected to MRI, or (iii) were treated with 4-MU for 24 h followed by the 2nd MRI session. For some experiments the unselective β receptor antagonist propranolol (0.5 mg/day) or the β3 adrenergic antagonist L-748,337 (100 μg/kg; Tocris Bioscience, Bristol, UK)[44] or respective vehicle control treatments were given either by drinking water (propranolol) or by i.p. 30 minutes prior to the application of 4-MU (L748,337 or respective vehicle). Efficacy of both β adrenergic receptor antagonists used was confirmed by complete inhibition of CL316,243-induced *Ucp1* mRNA expression in BAT. *Has2/3* double deficient mice and the respective wildtype control mice were measured without any additional BAT stimulation.

Blood and plasma analysis

Blood was drawn from the heart and was anti-coagulated with 100 mM ethylenediaminetetraacetic acid (EDTA) in isotonic sodium chloride solution. Plasma was collected after two centrifugation steps: at 800 × g for 15 minutes, and at 15,700 × g for 5 minutes at 4°C. Insulin concentration in plasma was analyzed by Ultra Sensitive Rat Insulin ELISA Kit (Crystal Chem, Inc, Downers Grove, IL, USA). Plasma leptin concentration was detected by an ELISA assay performed according to the manufacturer`s instructions

Europe PMC Funders Author Manuscripts

Europe PMC Funders Author Manuscripts

(Biotechne R&D Systems, Minneapolis, MN, USA). Cholesterol, HDL and VLDL + LDL cholesterol plasma concentration was determined by HDL and LDL/VLDL Quantification Colorimetric/Fluorometric Kit (Biovision, Inc., Milpitas, CA, USA). The concentration of triglycerides and nonesterified fatty acids (NEFA) in plasma was analyzed by Triglyceride Colorimetric Assay Kit (Cayman Chemical Company, Ann Arbor, MI, USA). Plasma non-esterified fatty acids (NEFA) were assessed photometrically using enzymatic kit (Autokit NEFA C, Wako, Neuss, Germany). Synergy Mx microplate reader and Gen5™ software (both BioTek, Berlin, Germany) were used for data analysis.

Liquid chromatography/tandem mass spectrometry (LC-MS/MS)

In order to determine circulating and tissue concentrations of 4-methylumbelliferone, plasma as well as white and brown adipose tissue (WAT, BAT) were harvested from mice treated for 24 hours with 4-MU or respective placebo. 4-methylumbelliferone was quantified in mice plasma by a liquid chromatography/tandem mass spectrometry (LC-MS/MS) method (lower limit of quantification: 0.00240 μg/mL for 4-methylumbelliferone).

The liquid chromatography system consisted of a binary LC-pump (Agilent 1200 Series, Agilent Technologies, Waldbronn, Germany) and an analytical column (Ascentis Express RP-Amide 4.6 x 50 mm 2.7 um, Sigma-Aldrich Chemie GmbH, Germany). Gradient elution was performed with 0.05% formic acid and acetonitrile. Determination was performed using an AB SCIEX API 5000 triple quadrupole mass spectrometer (AB SCIEX, Concord, Ontario, Canada) and Analyst software version 1.6.2 (AB SCIEX, Concord, Ontario, Canada). In brief, 10 μL of each sample was placed in a polypropylene-tube. Samples were deproteinized with 100 acetonitrile (containing the internal standard umbelliferone), subsequently vortex-shaked and centrifuged. The supernatant was further diluted with 0.05% formic acid and 30 μL for the mice plasma samples were injected into the LC-MS/MS system. The samples were detected with MRM (Multiple Reaction Monitoring) as follows: precursor → product ion for 4-methylumbelliferone 175.10 → 133.00 m/z, 4-methylumbelliferone-ß-glucuronide 351.20 → 174.90 m/z, 4-methylumbelliferyl-sulfate 255.30 → 175.00 m/z and for umbilliferone (internal standard) 161.00 → 133.00 m/z; for all analytes in negative mode. Under these conditions 4-methylumbelliferone, 4-methylumbelliferone-ß-glucuronide, 4-methylumbelliferyl-sulfate and umbilliferone eluted after approximately 1.3 minutes, 0.9 minutes, 1.5 minutes and 1.1 minutes, respectively.

Calibration standards and spiked quality controls samples (SQC) were prepared by adding a defined amount of analyte-solution to mice free plasma. Calibration was performed by weighted ($1/concentration^2$) linear regression.

Linearity for 4-methylumbelliferone could be demonstrated over a calibration range from 0.00240 to 0.299 μg/mL in mice plasma. No interferences were observed for 4-methylumbelliferone and the internal standard. The precision and accuracy for the 4-methylumbelliferone SQCs in mice plasma ranged from 4.2 to 5.6% and 101.1 to 104.2%.

4-Methylumbelliferone, concentrations were quantified in mice white epididymal AT by a liquid chromatography/tandem mass spectrometry (LC-MS/MS) method (lower limit of quantification in homogenate: 0.00174 μg/mL for 4-methylumbelliferone).

Europe PMC Funders Author Manuscripts

Europe PMC Funders Author Manuscripts

The homogenate of the tissue samples were analyzed as described for plasma. 20 mg of each tissue sample were homogenized with 300 acetonitrile (containing the internal standard umbelliferone). After homogenization the samples were vortex-shaked and centrifuged. The supernatant was further diluted with 0.05% formic acid and were injected into the LC-MS/MS system.

Calibration standards and spiked quality controls samples (SQC) were prepared by adding a defined amount of analyte-solution to mice free white epididymale AT. Calibration was performed by weighted ($1/concentration^2$) linear regression.

Linearity for 4-methylumbelliferone could be demonstrated over a calibration range from 1.67 to 188 μg/mL in mice white epididymale AT homogenate. No interferences were observed for 4-methylumbelliferone and the internal standard. The precision and accuracy for the 4-methylumbelliferone SQCs in mice white epididymale AT homogenate ranged from 1.1 to 2.8% and 96.4 to 101.4%. The precision and accuracy for the 4-methylumbelliferone SQCs in mice BAT homogenate ranged from 0.6 to 3.1% and 92.2 to 108.9%.

Immunohistochemical staining and determination of adipocyte size

Epididymal white adipose tissue (WAT) and interscapular brown adipose tissue (BAT) were removed and fixed for 24 hours in 4 % neutral buffered formalin, dehydrated and embedded in paraffin. For representative analysis of adipocyte size in white adipose tissue, tissue from three separate areas was cut into 5-μm sections. After the first sections had been collected, 300 μm of the tissue was discarded before the next sections were collected. This procedure was repeated again to obtain a total of three sections per object plate. White adipose tissue, brown adipose tissue, and liver sections (all 5 μm) were stained with hematoxylin and eosin (H&E). Adipocyte size in white adipose tissue was calculated from six pictures of different areas by using Fiji and Biovoxxel (Mutterstadt, Germany)[45]. Adipocyte area in BAT was calculated by using the AxioVision SE64 Rel. 4.8 software (Carl Zeiss Microscopy, Thornwood, NY, USA) as the mean area of a total of 50 cells per tissue. Staining with the uncoupling protein UCP-1 in brown adipose tissue was conducted with anti-UCP-1 primary antibody (1:500; ab10983, polyclonal, Lot GR130362-9, Abcam, Cambridge, UK) and goat anti-rabbit horseradish peroxidase (HRP)-coupled secondary antibody (1:200; sc-2004, LOT F2308, Santa Cruz Biotechnology, Dallas, TX, USA). Resident macrophages in white adipose tissue were stained with anti-Mac2 primary antibody (1:600; CL8942AP, clone M3/38, Lot 1442218A, Cedarlane, Burlington, Ontario, Canada) and goat anti-rat IgG2a HRP-coupled secondary antibody (1:600; nb7126, LOT P27, Novus Biologicals, Littleton, CO, USA). Macrophages were quantified by counting the number of Mac2-positive crown-like structures per 100 cells. For both UCP-1 and Mac2 stainings, diaminobenzidine (DAB) reagent was used for detection and hemalaun was used for staining of nuclei. Epitopes of α-galactose on endothelial cells in brown adipose tissue were bound by biotinylated isolectin B4 (1:100, Vector Laboratories, Burlingame, CA, USA), followed by staining with streptavidin-Cy5 (1:50, ZyMax™, Invitrogen™ by Thermo Fisher Scientific, Waltham, MO, USA). Nuclei were stained with Roti®-Mount FluorCare DAPI (Carl Roth GmbH & Co

KG, Karlsruhe). Validation of primary antibodies provided by/on the manufacturers' websites.

Respiration measurements in permeabilized BAT and isolated mitochondria

BAT was removed as described above. *Ex vivo* mitochondrial function was measured in fresh BAT using the Oxygraph-2k (Oroboros Instruments, Austria) as described before[46]. BAT was chemically permeabilized with digitonin. Defined respiratory states were obtained by the following protocol: 2 mmol/L malate, 10 mmol/L pyruvate (state 2, complex I), 10 mmol/L succinate (state 2, complex I+II), 2.5 mmol/L ADP (state 3, complex I+II), 10 µg/ml oligomycin (state 4o), carbonyl cyanide-p-trifluoromethoxyphenylhydrazone (stepwise increments of 0.25 mmol/L up to the final concentration of maximum 1.25 mmol/L, state u), and 2.5 mmol/L antimycin A. Data were normalized per tissue weight.

Citrate synthase activity (CSA), a marker of mitochondrial density, was assessed spectrophotometrically (Citrate Synthase Assay Kit, Sigma-Aldrich, St. Louis, MO, USA) and normalized to protein content measured with bicinchoninic acid assay.

To isolate mitochondria from BAT or beige adipose tissue, tissue was sliced in 1 mm thick pieces. BAT pieces were resuspended in 10 ml buffer I (0.3 M Sucrose, 10 mM HEPES (pH=7.2), 0.2 mM EDTA**)** and digested with trypsin (f.c. 0.06 mg/ml, Sigma, Deisenhofen, Germany, T8003) for 15 min at 4°C. During digestion each sample was further dispersed with an ULTRA-TURRAX (5 sec, level 6). After 15 min trypsin reaction was stopped with 5 ml trypsin-inhibitor (0.02 mg/ml, Sigma, T9128) in buffer II (0.25 M Sucrose, 20 mM HEPES (pH=7.4), 10 mM KCl, 1.5 mM MgCl2, 1 mM EDTA, 1 mM EGTA). Samples were centrifuged for 9 min at 800 x g 4°C. The supernatants were transferred into new tubes and centrifuged for 15 min at 10.000 x g 4°C. After centrifugation pellets were transferred into new tubes and centrifuged again for 5 min at 10.000 x g 4°C. Supernatant was entirely removed and resulting pellet was washed twice with buffer II and resuspended in buffer II. 250 - 500 µg mitochondria were used for respiration measurements with an OROBOROS 2k followed by data analysis using DatLab Software (OROBOROS instruments GmbH, Innsbruck, Austria) as described previously[47]. Defined respiratory states were obtained by the following protocol: 1 mmol/L malate and 1 mmol/l glutamate, 0.5 mmol/L (state 2 complex I) ADP (state 3 complex I), 0.4 nmol/L rotenone pyruvate (state 2, complex I),

Ex vivo glucose uptake into isolated mouse adipose cells

Epididymal fat pads were excised and pooled in 4 ml of Krebs Ringer bicarbonate HEPES (KRBH) buffer supplemented with 5% bovine serum albumin (BSA) and 2 mg/ml collagenase type I (Worthington Biochemical Corporation, Lakewood, NJ, USA). The fat pads were minced with scissors, and the suspension was shaken in a water bath at 160 rpm for 1 hour at 37° C. The cells were strained through a 400 µm sterile mesh and washed three times with KRBH buffer supplemented with 5 % BSA. Thereafter, cells were gently resuspended in KRBH buffer supplemented with 5 % BSA to yield a 6% cell suspension for the glucose uptake assay. Next, 200 µl of cell suspension was distributed to each vial containing 200 µl KRBH buffer supplemented with 5 % BSA with or without insulin and was then incubated for 30 minutes at 37° C in a gyratory bath. After the addition of 100 µl

Europe PMC Funders Author Manuscripts
Europe PMC Funders Author Manuscripts

Europe PMC Funders Author Manuscripts

Europe PMC Funders Author Manuscripts

hot medium with D-Glucose14C (U) (final concentration, 0.06 μCi/ml), cells were incubated for additional 30 minutes at 37°C. Glucose uptake was terminated by transferring 250 μl of the cell suspension to 100 μl of dinonyl phthalate (Merck KGaA, Darmstadt, Germany) in a microcentrifuge tube. The cells were centrifuged for 10 minutes at 10 000 rpm in the microcentrifuge. The cells (top layer) were cut away from the buffer (bottom layer) and transferred into scintillation tubes. Radioactivity was determined by scintillation counting. Each condition was assayed in five replicates.

An aliquot of the cell suspension from each group was taken before glucose uptake assay, and total lipids were extracted from these cells. Therefore, cell suspension was mixed with 2.7 ml extraction solution (80 % 2-propanol, 20 % N heptane, 2 % sulfuric acid) before the addition of 1.2 ml N heptane and 0.8 ml distilled water. Mixture was vortexed and centrifuged at 1000 rpm at room temperature for 5 minutes. Next, 1 ml of the organic phase was taken to a pre-weighed tube and dried with nitrogen, after which the tube with lipids was weighed again and the total lipid weight of the adipocytes was calculated. The counts per minute (CPM) values from the uptake assay were finally normalized to the corresponding lipid weight.

Cell culture

All results were confirmed in at least 3 independent experiments. The exact number of biological replicates is stated in the respective figure legend.

Primary murine preadipocytes—For isolation of murine preadipocytes from stromal vascular fraction of BAT, interscapular BAT from 4 – 5 mice was pooled to obtain 0.25 – 0.5 g of adipose tissue. Tissue was minced to a very fine consistency and digested with collagenase I (1000 U/ml) for 90 minutes at 37° C. After centrifugation for 5 minutes at 50 x g, the infranatant containing stromal vascular cells was collected and centrifuged for further 10 minutes at 200 x g. Erythrocyte lysis was performed for 5 minutes at room temperature. Afterwards, cell suspension was filtered through a 20 μm nylon mesh and centrifuged in a final step for 5 minutes at 200 x g. Pellet was resuspended and cells were seeded at a density of 50 000 cells / cm^2. Adipogenic differentiation was performed after cells had reached confluency. Differentiation of brown adipocytes was induced with 2 μg/ml dexamethasone, 5 μg/ml insulin, 125 μM indomethacin, 0.5 mM 3-isobutyl-1-methylxanthin (IBMX), 1 nM 3,3’,5-triiodo-L-thyronine (T3) and 0.5 μM rosiglitazone (all substances obtained from Sigma Aldrich, St. Louis, MO, USA). After 2 days, maintenance medium containing 5 μg/ml insulin and 1 nM T3 was added and henceforth changed every 2 – 3 days. For brown adipocyte culture and differentiation, Dulbecco’s modified Eagle’s Medium (DMEM) supplemented with 4.5 g/l glucose and 10 % fetal calf serum (FCS; GibcoBRL, Rockville, MD, USA) was utilized.

Primary human preadipocytes—For human preadipocytes, the stromal vascular fraction was obtained using collagenase digestion from brown adipose tissue from four female patients undergoing deep neck surgery (Age: 48, 55, 19, 34 years; procedure: hemithyroidectomy, hemithyroidectomy, lymph node excision, lymph node excision, respectively). The protocol was reviewed and approved by the ethics committee of

Europe PMC Funders Author Manuscripts

Europe PMC Funders Author Manuscripts

Maastricht University Medical Center (METC 10-3-012, NL31367.068.10; ClinicalTrials.gov identifier: NCT03111719) and all procedure complied with the relevant ethical regulations. Informed consent was obtained before surgery. Inclusion criteria included: indication for surgery in the supraclavicular and neck region (more specific patients diagnosed with hyperparathyroidism, struma, benign thyroid gland tumours, implantation of a vagal neurostimulator for epilepsia and cervical neurologic disorders); in the thyroid gland group, euthyroid function. Exclusion criteria were: pre-operatively diagnosed malign tumour and patients undergoing acute surgery because of critical illness. Collected cells were grown in DMEM/F12 medium supplemented with 10 % FBS and antibiotics to confluence before differentiation was initiated. Differentiation was initiated for 7 days via differentiation medium containing biotin (33 mM), pantothenate (17 mM), insulin (100 nM), dexamethasone (100 nM), IBMX (250 mM), rosiglitazone (5 mM), T3 (2 nM), and transferrin (10 mg/ml). Cells were transferred to maintenance medium consisting of biotin (33 mM), pantothenate (17 mM), insulin (100 nM), dexamethasone (10 nM), T3 (2 nM), and transferrin (10 mg/ml) until lipid-rich adipocytes had formed. During the entire differentiation process, cell media was replaced every other day.

For incubations with 4MU, in vitro differentiated adipocytes were incubated for 24 h with the 100 μM 4-MU (4-Methylumbelliferone sodium salt; Sigma Aldrich) in plain DMEM/F12 medium. Adipocytes were washed with PBS and harvested in trizol.

Lactate-Assay—After excluding mycoplasma contamination, T37i brown preadipocytes, kindly provided by Marc Lombes[48], were incubated with 100 μM 4-MU or lactate in the indicated concentrations for 24 h as described above. As a positive control cells were incubated with the complex I inhibitor rotenone (2 μM; Sigma Aldrich) for 4h. Afterwards, cells were harvested and the lactate assay was performed according to the manufacturers protocol (Sigma Life Science, St. Louis, MO, USA).

Western blots

For Western blots, 20 mg BAT tissue were homogenized in 200 μl modified RIPA buffer (150 mM NaCl, 50 mM Tris/HCl pH 7.4, 1% Nonidet-P40, 0.5% sodium deoxycholate, 0.1% SDS, 2 mM PMSF). Homogenates were centrifuged at 4°C, 10 000 x g for 10 min. The top fat layer was descarded and the lysate was mixed with an equal amount of reducing sample buffer. For protein determination 100 mg BAT tissue were lysed in 200 μl RIPA buffer (25 mM Tris/HCl, 140 mM NaCl, 1% triton X100, 0,5% SDS, 1 mMEDTA, pH 7,4 1 mM NaF, 1 mM β-Glycerophosphat, 150 nM Aprotinin, 1 mM PMSF) and mechanical disrupted using FastGene Tissue Grinder NG010 (NIPPON Genetics EUROPE) for 15 seconds. After a centrifugation step (10000 x g, 10 minutes, 4°C) the fat layer was discarded. Protein concentration was determined using the BCA Assay Kit (Thermo Scientific #23227).

Proteins were separated by SDS-PAGE and transferred to PVDF (polyvinyliden difluoride membrane, GE Healthcare Life Sciences) using a semi-dry electrophoretic transfer cell. For the western blot of total oxphos SDS-PAGE was performed using a gradient gel (5-20% SDS) followed by treansfer to a nitrocellulose membrane using a semi-dry electrophoretic

Europe PMC Funders Author Manuscripts

Europe PMC Funders Author Manuscripts

transfer cell, After blocking in Odyssey® Blocking Buffer (TBS) (LI-COR), anti-tyrosine hydroxylase antibody (ab112, polyclonal, Lot GR286793-17, Abcam), total OXPHOS Rodent WB Antibody Cocktail (Abcam, ab110413), HSL Antibody (Cell Signaling, #4107, Lot 3, Danvers, MA, USA) or anti-UCP1 antibody (ab10983, polyclonal, Lot GR249119-7, Abcam) were used in a dilution of 1:1,000 at 4° C o/n, anti-β-tubulin I (T7816, clone SAP. 4G5, Lot 025M4776V, Sigma-Aldrich, St. Louis, MO, USA) 1:10,000 at RT for 1 h. Immunoblots were visualized by infrared fluorescent-coupled secondary antibodies (Goat anti-mouse IRDye® 800CW, 926-32210, LOT C40826-01; Goat anti-rabbit IRDye® 800CW, 926-32211, LOT C50331-05; Goat anti-mouse IRDye® 680LT, 926-68020 LOT C50113-11; all LI-COR Biosciences, Lincoln, NE, USA) allowing fluorescent detection on a LI-COR Odyssey infrared imaging system using Odyssey application software version 3.0 (both LI-COR). Validation of the antibodies is provided by the manufacturer.

RNA analysis

RNA from cells and tissue was isolated with peqGOLD TriFast (PEQLAB Biotechnologie GmbH, Erlangen, Germany). RNA concentration and quality was determined via photometric measurement at absorbance 260/280 nm (Nanodrop ND1000, PeqLab, Erlangen, Germany). 1000 ng of RNA was transcribed into cDNA with the QuantiTect Reverse Transcription Kit (Qiagen, Hilden, Germany). For analysis of mRNA expression the Applied Biosystems 7300 Real-Time PCR System with the Sequence Detection Software Version 1.4 (Applied Biosystems, Foster City, CA, USA) or the StepOnePlus Real-Time PCR System with StepOne Software v2.3 and SYBR Green PCR master mix (Life Technologies Thermo Fisher Scientific, Waltham, MA, USA) were used. Primers used in quantitative real-time polymerase chain reaction (qPCR) were designed with the help of Primer3Plus Software (Free Software Foundation, Boston, MA, USA)[49] and NCBI Primer Blast (National center for biotechnology information, Bethesda, MD, USA)[50]; respective sequences are listed in the Supplementary Table 1 and 2. Quantification of qPCR was performed by the ΔΔCq method. All values are normalized to the expression of 18S.

Statistics and Reproducibility

Sample size estimation was based upon our own previous results in comparable studies, assuming to achieve 90% power at a significance level of 0.05. If applicable, mice were allocated into experimental groups by randomization. Specifications of how many independent biological samples/animals were included in the experiment or how many times experiments were repeated independently are given in the respective figure legend.

GraphPad Prism 7 software was used for analysis of statistical significance. All data are presented as means ± standard error of the mean (SEM), unless otherwise indicated. Values identified as outliers by Grubbs' test ($\alpha = 0.05$) were excluded from analysis. Sample size for each experiment and statistical tests used are indicated in the respective figure legend. For comparison of two independent groups unpaired two-tailed Student`s *t*-tests or Mann-Whitney test were used. Repeated measurements in the same mouse were analyzed by paired Student`s *t*-tests. Comparison of more than two groups was performed using One-way ANOVA with Sidak`s post-hoc test, or Two-way ANOVA with Sidak`s post-hoc test. Statistical testing for qPCR results was performed with log-transformed data. Statistical

Europe PMC Funders Author Manuscripts

Europe PMC Funders Author Manuscripts

significance was set at the level of $P < 0.05$. Only significant results are stated in the respective figures as exact values.

Supplementary Material

Refer to Web version on PubMed Central for supplementary material.

Acknowledgements

Marc Lombes (INSERM U-1185, UMS-32 Institut Biomedical de Bicetre I2B Faculte de Medecine Paris Sud 63, rue Gabriel Peri 94276 Le Kremlin-Bicetre Cedex, France) kindly provided the T37I cell line.

We also thank Annika Zimmermann, Petra Rompel, Irmhild Rüter and Kerstin Freidel for excellent technical assistance.

All animal work was carried out in the Disease Model Core (MRC Metabolic Diseases Unit [MRC_MC_UU_12012/5]. We thank the BHF [RG/12/13/29853] and MRC [MC_UU_12012/2] for funding this work.

This study was supported in part by the German Research Foundation (DFG; IRTG 1902, SFB1116), the Ministry of Science and Research of the State of North Rhine-Westphalia (MIWF NRW), the German Federal Ministry of Health (BMG), a grant from the Federal Ministry for Research (BMBF) to the German Center for Diabetes Research (DZD e.V.; DZD Grant 2012), and by grants from the Helmholtz portfolio (theme: Metabolic Dysfunction and Common Disease), the Helmholtz Alliance to Universities: Imaging and Curing Environmental Metabolic Diseases (ICEMED) and the Research Training Group **vivid**.

References

1. Cypess AM, et al. Identification and importance of brown adipose tissue in adult humans. N Engl J Med. 2009; 360:1509–1517. [PubMed: 19357406]
2. Virtanen KA, et al. Functional brown adipose tissue in healthy adults. N Engl J Med. 2009; 360:1518–1525. [PubMed: 19357407]
3. Hondares E, et al. Thermogenic activation induces FGF21 expression and release in brown adipose tissue. J Biol Chem. 2011; 286:12983–12990. [PubMed: 21317437]
4. Bartelt A, et al. Brown adipose tissue activity controls triglyceride clearance. Nat Med. 2011; 17:200–205. [PubMed: 21258337]
5. Orava J, et al. Different metabolic responses of human brown adipose tissue to activation by cold and insulin. Cell Metab. 2011; 14:272–279. [PubMed: 21803297]
6. Guerra C, Koza RA, Yamashita H, Walsh K, Kozak LP. Emergence of brown adipocytes in white fat in mice is under genetic control. Effects on body weight and adiposity. J Clin Invest. 1998; 102:412–420. [PubMed: 9664083]
7. Lee P, et al. Temperature-acclimated brown adipose tissue modulates insulin sensitivity in humans. Diabetes. 2014; 63:3686–3698. [PubMed: 24954193]
8. Collaboration, T.G.B.M. et al. Body-mass index and all-cause mortality: individual-participant-data meta-analysis of 239 prospective studies in four continents. Lancet. 2016; 388:776–786. [PubMed: 27423262]
9. Berbee JF, et al. Brown fat activation reduces hypercholesterolaemia and protects from atherosclerosis development. Nature communications. 2015; 6
10. Shimizu I, et al. Vascular rarefaction mediates whitening of brown fat in obesity. J Clin Invest. 2014; 124:2099–2112. [PubMed: 24713652]
11. Stanford KI, et al. Brown adipose tissue regulates glucose homeostasis and insulin sensitivity. J Clin Invest. 2013; 123:215–223. [PubMed: 23221344]
12. Cypess AM, et al. Activation of human brown adipose tissue by a beta3-adrenergic receptor agonist. Cell Metab. 2015; 21:33–38. [PubMed: 25565203]

Europe PMC Funders Author Manuscripts

13. Bortolini M, Wright MB, Bopst M, Balas B. Examining the safety of PPAR agonists - current trends and future prospects. Expert Opin Drug Saf. 2013; 12:65–79. [PubMed: 23134541]
14. Camporez JP, et al. Cellular mechanisms by which FGF21 improves insulin sensitivity in male mice. Endocrinology. 2013; 154:3099–3109. [PubMed: 23766126]
15. van Marken Lichtenbelt WD, et al. Cold-activated brown adipose tissue in healthy men. N Engl J Med. 2009; 360:1500–1508. [PubMed: 19357405]
16. Vijgen GH, et al. Brown adipose tissue in morbidly obese subjects. PLoS One. 2009; 6:e17247.
17. Vigetti D, et al. Role of UDP-N-acetylglucosamine (GlcNAc) and O-GlcNAcylation of hyaluronan synthase 2 in the control of chondroitin sulfate and hyaluronan synthesis. J Biol Chem. 2012; 287:35544–35555. [PubMed: 22887999]
18. Kang L, et al. Hyaluronan accumulates with high-fat feeding and contributes to insulin resistance. Diabetes. 2013; 62:1888–1896. [PubMed: 23349492]
19. Lee P, et al. Brown Adipose Tissue Exhibits a Glucose-Responsive Thermogenic Biorhythm in Humans. Cell Metab. 2016; 23:602–609. [PubMed: 26972823]
20. Kakizaki I, et al. A novel mechanism for the inhibition of hyaluronan biosynthesis by 4-methylumbelliferone. J Biol Chem. 2004; 279:33281–33289. [PubMed: 15190064]
21. Peirce V, Carobbio S, Vidal-Puig A. The different shades of fat. Nature. 2014; 510:76–83. [PubMed: 24899307]
22. Chondronikola M, et al. Brown adipose tissue improves whole-body glucose homeostasis and insulin sensitivity in humans. Diabetes. 2014; 63:4089–4099. [PubMed: 25056438]
23. De Meis L, Ketzer LA, Camacho-Pereira J, Galina A. Brown adipose tissue mitochondria: modulation by GDP and fatty acids depends on the respiratory substrates. Biosci Rep. 2012; 32:53–59. [PubMed: 21561434]
24. Vigetti D, Viola M, Karousou E, De Luca G, Passi A. Metabolic control of hyaluronan synthases. Matrix Biol. 2014; 35:8–13. [PubMed: 24134926]
25. Carriere A, et al. Browning of white adipose cells by intermediate metabolites: an adaptive mechanism to alleviate redox pressure. Diabetes. 2014; 63:3253–3265. [PubMed: 24789919]
26. Hui S, et al. Glucose feeds the TCA cycle via circulating lactate. Nature. 2017; 551:115–118. [PubMed: 29045397]
27. Blondin DP, et al. Inhibition of Intracellular Triglyceride Lipolysis Suppresses Cold-Induced Brown Adipose Tissue Metabolism and Increases Shivering in Humans. Cell metabolism. 2017; 25:438–447. [PubMed: 28089568]
28. Irshad Z, Dimitri F, Christian M, Zammit VA. Diacylglycerol acyltransferase 2 links glucose utilization to fatty acid oxidation in the brown adipocytes. Journal of lipid research. 2017; 58:15–30. [PubMed: 27836993]
29. De Bock K, et al. Role of PFKFB3-driven glycolysis in vessel sprouting. Cell. 2013; 154:651–663. [PubMed: 23911327]
30. Mahdaviani K, Chess D, Wu Y, Shirihai O, Aprahamian TR. Autocrine effect of vascular endothelial growth factor-A is essential for mitochondrial function in brown adipocytes. Metabolism. 2016; 65:26–35. [PubMed: 26683794]
31. Sim MO, Ham JR, Lee HI, Seo KI, Lee MK. Long-term supplementation of umbelliferone and 4-methylumbelliferone alleviates high-fat diet induced hypertriglyceridemia and hyperglycemia in mice. Chem Biol Interact. 2014; 216:9–16. [PubMed: 24661945]
32. Ji E, et al. Inhibition of adipogenesis in 3T3-L1 cells and suppression of abdominal fat accumulation in high-fat diet-feeding C57BL/6J mice after downregulation of hyaluronic acid. Int J Obes (Lond). 2014; 38:1035–1043. [PubMed: 24173405]
33. Chen YI, et al. Anatomical and functional assessment of brown adipose tissue by magnetic resonance imaging. Obesity (Silver Spring). 2012; 20:1519–1526. [PubMed: 22343821]
34. Khanna A, Branca RT. Detecting brown adipose tissue activity with BOLD MRI in mice. Magn Reson Med. 2012; 68:1285–1290. [PubMed: 22231619]
35. Quaranta S, Rossetti S, Camarri E. [Double-blind clinical study on hymecromone and placebo in motor disorders of the bile ducts after cholecystectomy]. Clin Ter. 1984; 108:513–517. [PubMed: 6233070]

Europe PMC Funders Author Manuscripts

36. Abate A, et al. Hymecromone in the treatment of motor disorders of the bile ducts: a multicenter, double-blind, placebo-controlled clinical study. Drugs Exp Clin Res. 2001; 27:223–231. [PubMed: 11951580]
37. Trabucchi E, et al. Controlled study of the effects of tiropramide on biliary dyskinesia. Pharmatherapeutica. 1986; 4:541–550. [PubMed: 2429334]
38. Kobayashi N, et al. Hyaluronan deficiency in tumor stroma impairs macrophage trafficking and tumor neovascularization. Cancer Res. 2010; 70:7073–7083. [PubMed: 20823158]
39. Matsumoto K, et al. Conditional inactivation of Has2 reveals a crucial role for hyaluronan in skeletal growth, patterning, chondrocyte maturation and joint formation in the developing limb. Development. 2009; 136:2825–2835. [PubMed: 19633173]
40. Seibler J, et al. Rapid generation of inducible mouse mutants. Nucleic Acids Res. 2003; 31:e12. [PubMed: 12582257]
41. Kiene LS, et al. Deletion of Hyaluronan Synthase 3 Inhibits Neointimal Hyperplasia in Mice. Arterioscler Thromb Vasc Biol. 2016; 36:e9–16. [PubMed: 26586662]
42. Flogel U, Jacoby C, Godecke A, Schrader J. In vivo 2D mapping of impaired murine cardiac energetics in NO-induced heart failure. Magn Reson Med. 2007; 57:50–58. [PubMed: 17139621]
43. Vegiopoulos A, et al. Cyclooxygenase-2 controls energy homeostasis in mice by de novo recruitment of brown adipocytes. Science. 2010; 328:1158–1161. [PubMed: 20448152]
44. Aragon JP, et al. Beta3-adrenoreceptor stimulation ameliorates myocardial ischemia-reperfusion injury via endothelial nitric oxide synthase and neuronal nitric oxide synthase activation. J Am Coll Cardiol. 2011; 58:2683–2691. [PubMed: 22152956]
45. Schindelin J, et al. Fiji: an open-source platform for biological-image analysis. Nat Methods. 2012; 9:676–682. [PubMed: 22743772]
46. Jelenik T, et al. Tissue-specific differences in the development of insulin resistance in a mouse model for type 1 diabetes. Diabetes. 2014; 63:3856–3867. [PubMed: 24917575]
47. Haendeler J, et al. Mitochondrial telomerase reverse transcriptase binds to and protects mitochondrial DNA and function from damage. Arterioscler Thromb Vasc Biol. 2009; 29:929–935. [PubMed: 19265030]
48. Zennaro MC, et al. Hibernoma development in transgenic mice identifies brown adipose tissue as a novel target of aldosterone action. J Clin Invest. 1998; 101:1254–1260. [PubMed: 9502766]
49. Untergasser A, et al. Primer3Plus, an enhanced web interface to Primer3. Nucleic Acids Res. 2007; 35:W71–74. [PubMed: 17485472]
50. Ye J, et al. Primer-BLAST: a tool to design target-specific primers for polymerase chain reaction. BMC Bioinformatics. 2012; 13:134. [PubMed: 22708584]

Europe PMC Funders Author Manuscripts

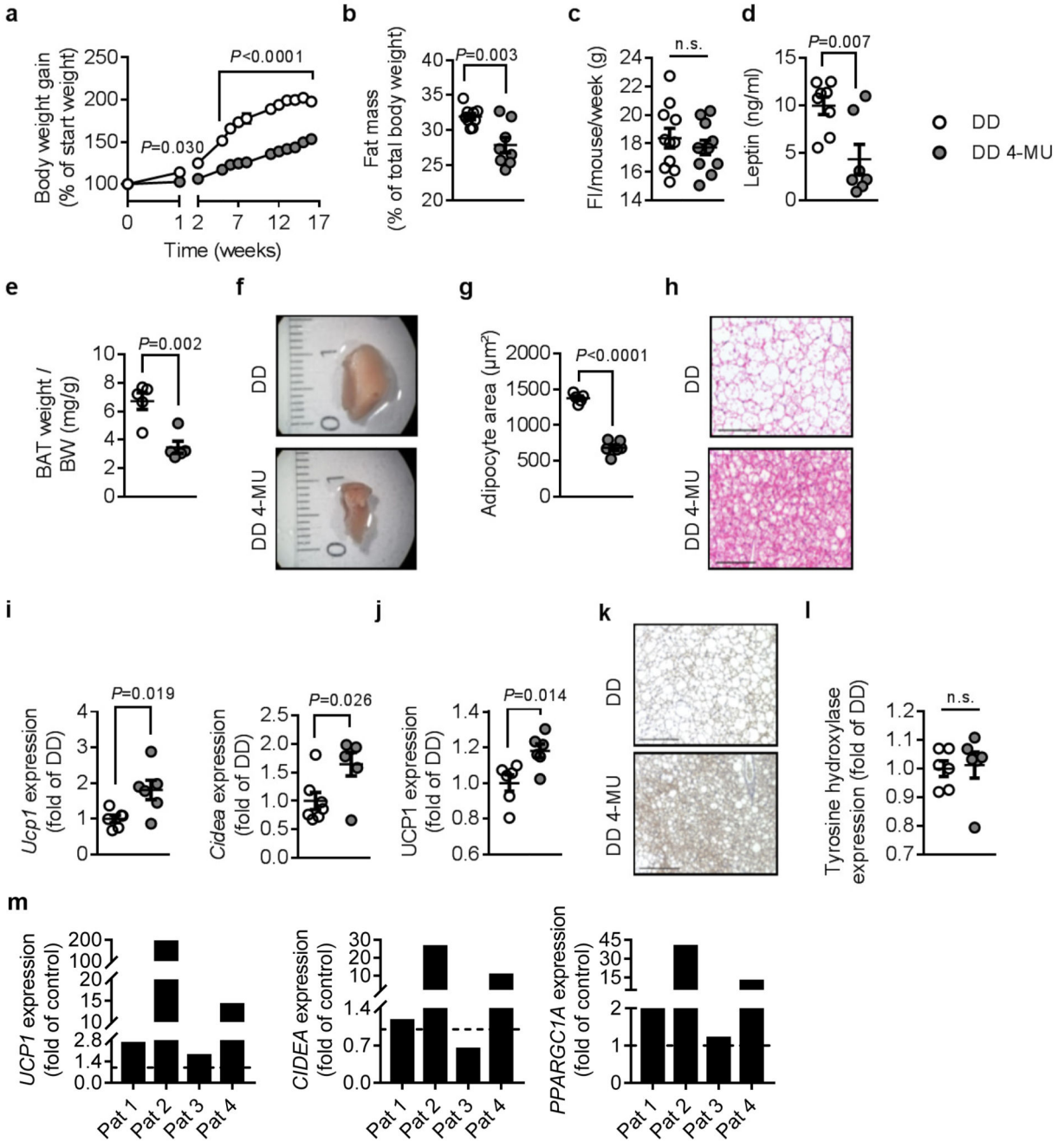

Figure 1. 4-MU prevents diet-induced obesity and increases markers of brown adipose tissue (BAT) activation in mice and humans.

(**a**) Body weight gain of male C57BL/6J mice after start of feeding diabetogenic diet (DD) supplemented with or without 4-MU at 8-10 weeks of age; n = 8 (DD),8 (DD 4-MU) mice; except week 3 + 4: n = 7,6 mice; week 9 + 10: n = 5,6 mice. (**b**) Percentage of body fat (n = 9,8 mice) after 17 weeks of feeding and (**c**), food intake (FI) per mouse per week during the first 11 weeks of feeding; n = 11,11 mice. After 22 weeks of feeding either DD or DD 4-MU the following parameters were analyzed: (**d**) plasma leptin; n = 8,7 biologically independent

Europe PMC Funders Author Manuscripts
Europe PMC Funders Author Manuscripts

Europe PMC Funders Author Manuscripts

Europe PMC Funders Author Manuscripts

samples; (**e**) BAT weight corrected for body weight (BW); and (**f**) representative images of the right BAT lobe from n = 5,5 biologically independent samples. (**g**) Quantification of brown adipocyte area and (**h**) respective representative H&E staining of BAT from n = 5,6 biologically independent samples. (**i**) BAT *Ucp1* (n = 6,6 biologically independent samples) and *Cidea* (n = 7,6 biologically independent samples) mRNA expression as determined by qPCR. (**j**) UCP1 protein expression in BAT normalized to β-tubulin; n = 6,6 biologically independent samples. (**k**) Representative images of BAT UCP1 staining after 17 weeks of feeding DD or DD 4-MU from n = 6,6 independent biological samples respectively. (**l**) Tyrosin hydroxylase protein expression in BAT normalized to β-tubulin; n = 6,6 biologically independent samples. (**m**) *UCP1, CIDEA,* and *PPARGC1A* mRNA expression, as determined by qPCR, in human differentiated brown preadipocytes isolated from 4 patients (Pat) and treated with 4-MU (100 μM) or respective vehicle (control) for 24 h. Scale bars indicate 100 μm (**h**) and 200 μm (**k**). Data are presented as means ± s.e.m.. (**a**) Two-way ANOVA with post hoc Sidak`s multiple comparison test; *P:* DD 4-MU versus DD; (**b**) Mann-Whitney test or (**c**, **d**, **e**, **g**, **i**, **j, l**) two-tailed unpaired Student's *t*-test. n.s.: not significant.

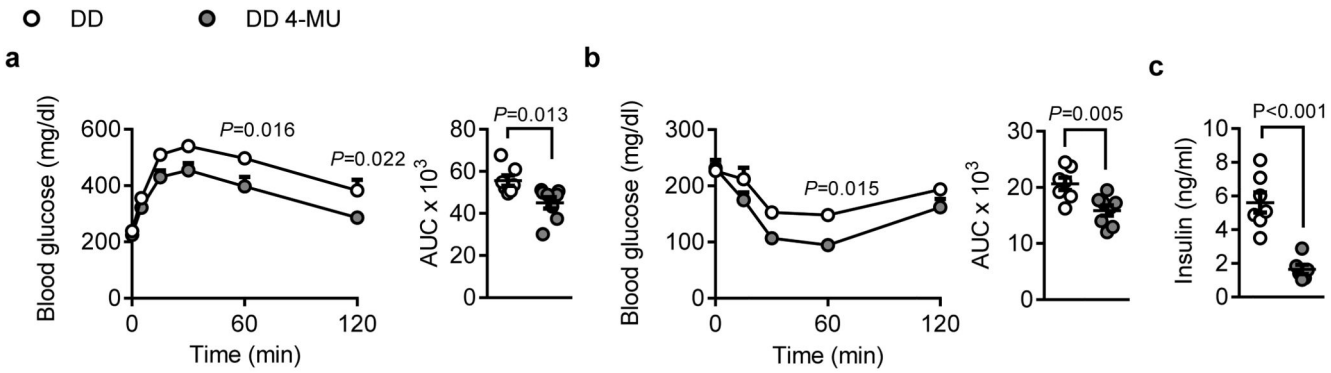

Figure 2. 4-MU treatment improves insulin sensitivity.

(**a**) Intraperitoneal glucose tolerance test performed after 13 weeks of feeding diabetogenic diet (DD) supplemented with or without 4-MU in male C57BL/6J mice; n = 7,8. Absolute values of blood glucose concentration (left) at 0, 5, 15, 30, 60, and 120 minutes, and respective area under the curve (AUC; right) are shown. (**b**) Insulin tolerance test performed after 14 weeks of feeding; n = 8,8 biologically independent samples. Absolute values of blood glucose concentration (left) at 0, 15, 30, 60, and 120 minutes, and respective area under the curve (AUC; right) are shown. (**c**) Fasting plasma insulin concentrations measured after 22 weeks of feeding; n = 7,6 biologically independent samples. Data are presented as means ± s.e.m.. (**a, b** left) Two-way ANOVA with post hoc Sidak`s multiple comparison test, *P:* DD 4-MU versus DD; (**a**, **b** right, **c**) two-tailed unpaired Student's *t*-test.

Europe PMC Funders Author Manuscripts
Europe PMC Funders Author Manuscripts

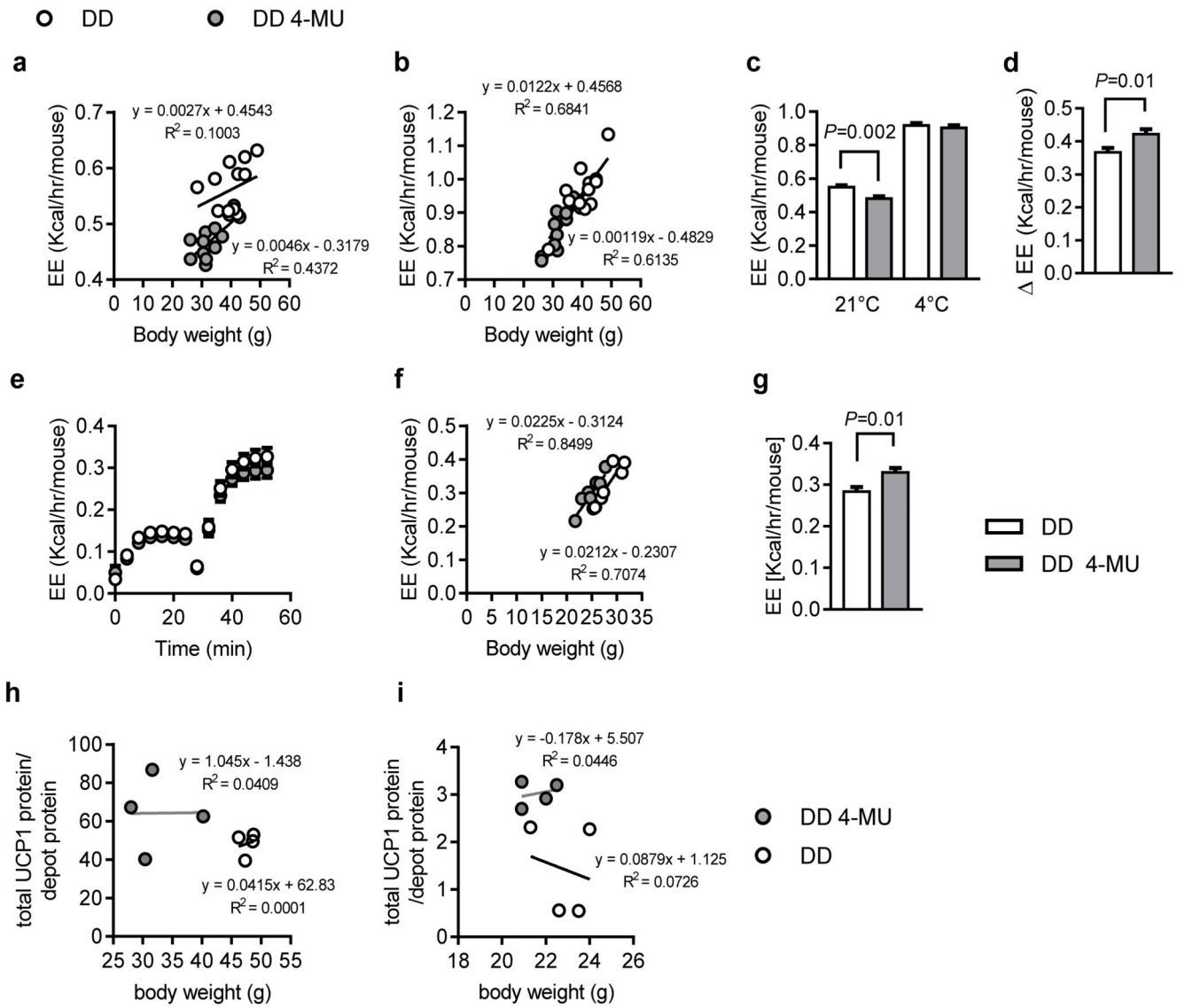

Figure 3. 4-MU increases BAT`s thermogenic capacity.

Male, 8-week-old C57BL/6J mice were fed diabetogenic diet (DD) supplemented with or without 4-MU (DD 4-MU) for 11 weeks followed by energy expenditure (EE) assessment at (**a**) 21°C and (**b**) 4°C; n = 13 DD, n = 11 DD 4-MU mice. (**c**) EE at 21°C and 4°C and (**d**), the delta Δ increase in EE for 21°C versus 4°C corrected for body weight using ANCOVA. Data are presented as means ± s.e.m.. Covariates assessed at BW = 36.6 g. n = 13 DD, n = 11 DD 4-MU mice. (**e-g**). After 4 weeks of feeding DD supplemented without or with 4-MU (DD 4-MU), maximum thermogenic capacity was assessed after injection of 1 mg/kg norepinephrine subcutaneously followed by measurement of the EE. Data are presented as (**e**) uncorrected EE, (**f**) uncorrected EE plotted against body weight, (**g**) EE corrected for body weight by ANCOVA covariates assessed at BW = 26.4 g ± s.e.m.; n = 7 (DD), 8 (DD 4-MU) mice for thermogenic capacity. Data are presented as means ± s.e.m.. After (**h**) 11 weeks of feeding either DD or DD 4-MU, n = 4,4 biologically independent samples, or (**i**)

Europe PMC Funders Author Manuscripts
Europe PMC Funders Author Manuscripts

24 hours of 4-MU treatment, body and BAT weight were measured and BAT protein lysates were used to detect UCP1 expression, n = 4,4 biologically independent samples. Total amounts of UCP1 protein were calculated per BAT depot according to the calculations described by Kalinovich *et al.,* Biochimie 2017. (**a**, **b**, **f**, **h**, **i**) linear regression, (**c**) one-way ANOVA with Sidak`s multiple comparison test, (**d**, **g**) unpaired Student's *t*-test.

Europe PMC Funders Author Manuscripts

Europe PMC Funders Author Manuscripts

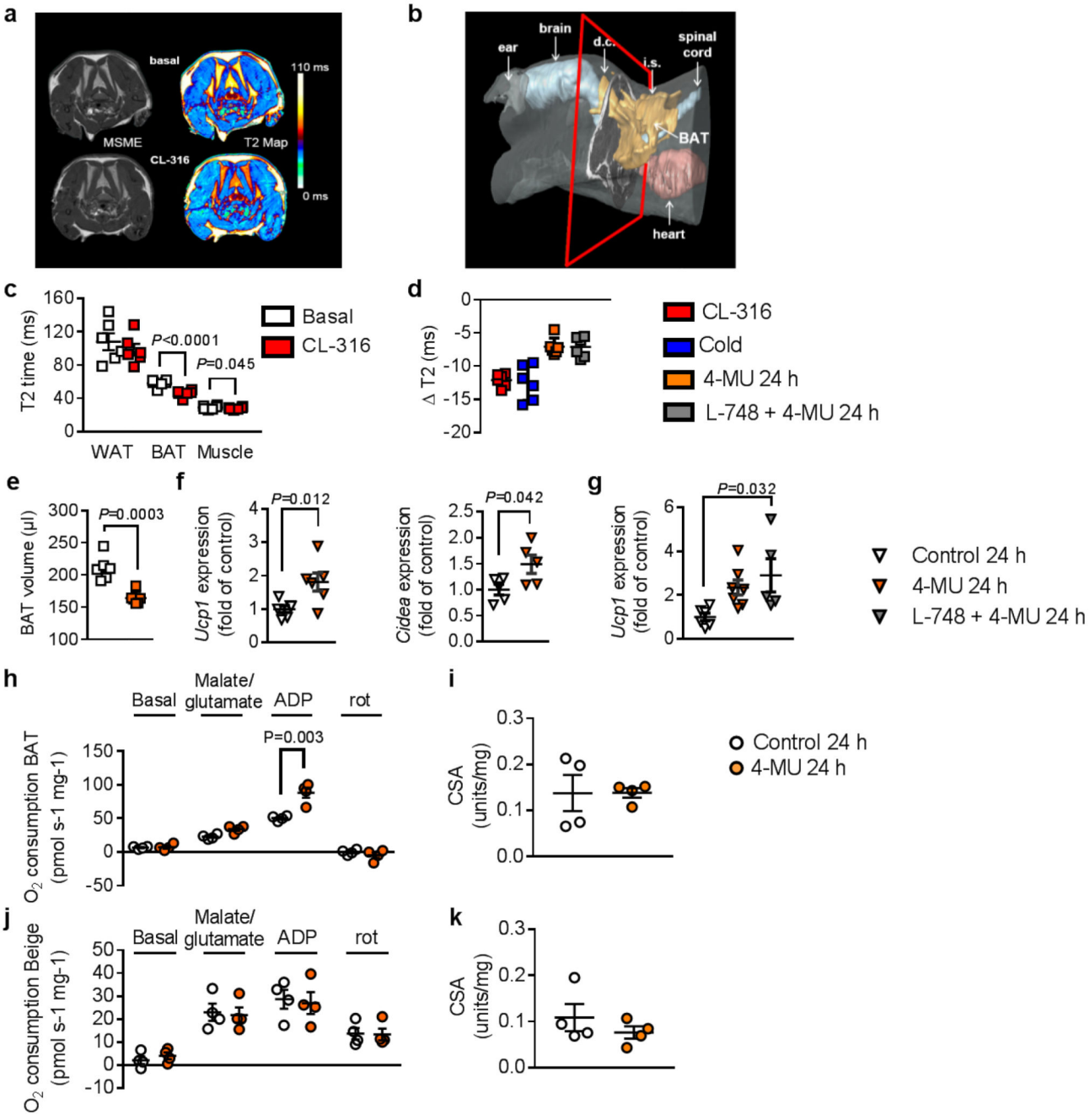

Figure 4. Acute 4-MU treatment increases respiration and mitochondrial complex I activity in brown adipose tissue (BAT).

(**a**) *In vivo* visualization of β3 agonist CL-316,243 (CL-316; 1 mg/kg intraperitoneal (i.p.); 1 h)-induced BAT activation by T2 maps (right) calculated from multi-slice multi-echo (MSME) magnetic resonance images (MRI, left) from 3 independently repeated experiments in C57BL/6J mice at 8-10 weeks of age. (**b**) Reconstruction of a 3D MR dataset illustrating shape and localization of BAT in the mouse torso showing the interconnection of interscapular (i.s.) and dorsocervical (d.c.) brown fat depots (cf. Supplementary video) from

Europe PMC Funders Author Manuscripts
Europe PMC Funders Author Manuscripts

3 independently repeated experiments. Red borders specify MR slice positionings in (a). (**c**) Quantification of T2 values for white adipose tissue (WAT), BAT, and skeletal muscle before and 1 h after CL-316 stimulation; n = 6 mice. (**d**) Compilation of T2 decrease (ΔT2) in BAT after exposure of mice to CL-316, cold (4°C), 4-MU, and the β3 antagonist L-748,337 (L-748; 100 μg/kg), respectively (n = 6 mice). (**e**) Decrease in total BAT volume after 24 h of 4-MU administration as determined from multi-slice MRI datasets; n = 6 mice. (**f**) Increased mRNA expression of BAT activation markers *Ucp1* (n = 6 biologically independent samples) and *Cidea* (n = 5 biologically independent samples) after 24 h of 4-MU treatment. (**g**) *Ucp1* mRNA expression in BAT from mice treated for 24 h with 4-MU alone or in combination with L-748 or respective control; n = 6,7,5 biologically independent samples. Complex I respiration was measured in isolated mitochondria from (**h**) BAT and (**j**) inguinal adipose after 24 h of treatment with 4-MU or respective control using an OROBOROS 2k; n = 4 biologically independent samples. Citrate synthase activity (CSA) in (**i**) BAT and (**k**) inguinal AT was measured as a marker of mitochondrial density (n = 4 biologically independent samples) after 24 h of treatment with 4-MU or respective control. Data are presented as means ± s.e.m. (except (**e**): means ± s.d.). (**c**) Paired Student's *t*-test, (**e**, **f**, **h**, **i**, **j**) two-tailed unpaired Student's *t*-test or (**g**) one-way ANOVA with post hoc Sidak´s multiple comparison test. rot: rotenone.

Europe PMC Funders Author Manuscripts

Europe PMC Funders Author Manuscripts

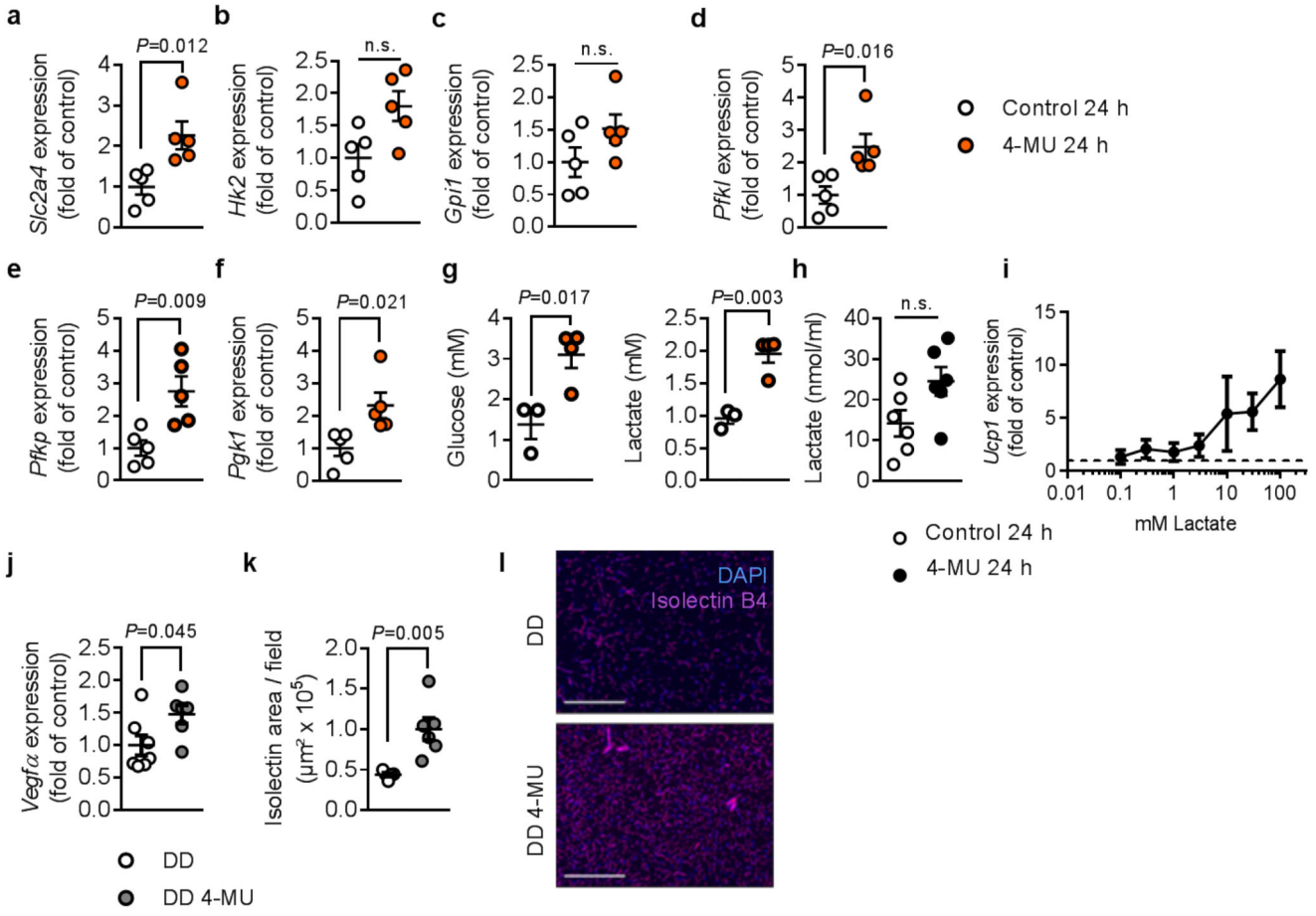

Figure 5. 4-MU increases glycolysis and vascularization in brown adipose tissue (BAT).

Increased mRNA expression of (**a-f**) glycolytic enzymes in BAT of C57BL/6J mice after 24 h treatment with 4-MU or respective control; n = 5,5 biologically independent samples. (**g**) Mice were treated for 24 h with 4-MU or respective control, followed by detection of glucose and lactate concentrations in BAT by high-resolution ^{1}H magnetic resonance (MR) spectroscopy; n = 6,8 biologically independent samples (BAT of two mice pooled in each sample). (**h**) Measurement of lactate concentrations in T37i brown preadipocytes after 24 h of 4-MU (100 µM) treatment; n = 6,6 biologically independent samples. (**i**) *Ucp1* mRNA expression after stimulation of T37i cells with increasing concentrations of lactate for 24 h (n = 4 biologically independent samples). Dashed line indicating control level (=1). (**j**) *Vegfa* mRNA expression in BAT from mice treated for 22 weeks with DD or DD 4-MU; n = 7,6 biologically independent samples. (**k**) Quantification and (**l**) representative pictures of isolectin B4 staining of BAT from n = 5,6 biologically independent samples are shown. Scale bars indicate 200 µm; Data are presented as means ± s.e.m.. (**a-h**, **j**, **k**) Two-tailed unpaired Student's *t*-test or (**k**) Mann-Whitney test. n.s.: not significant.

Europe PMC Funders Author Manuscripts
Europe PMC Funders Author Manuscripts

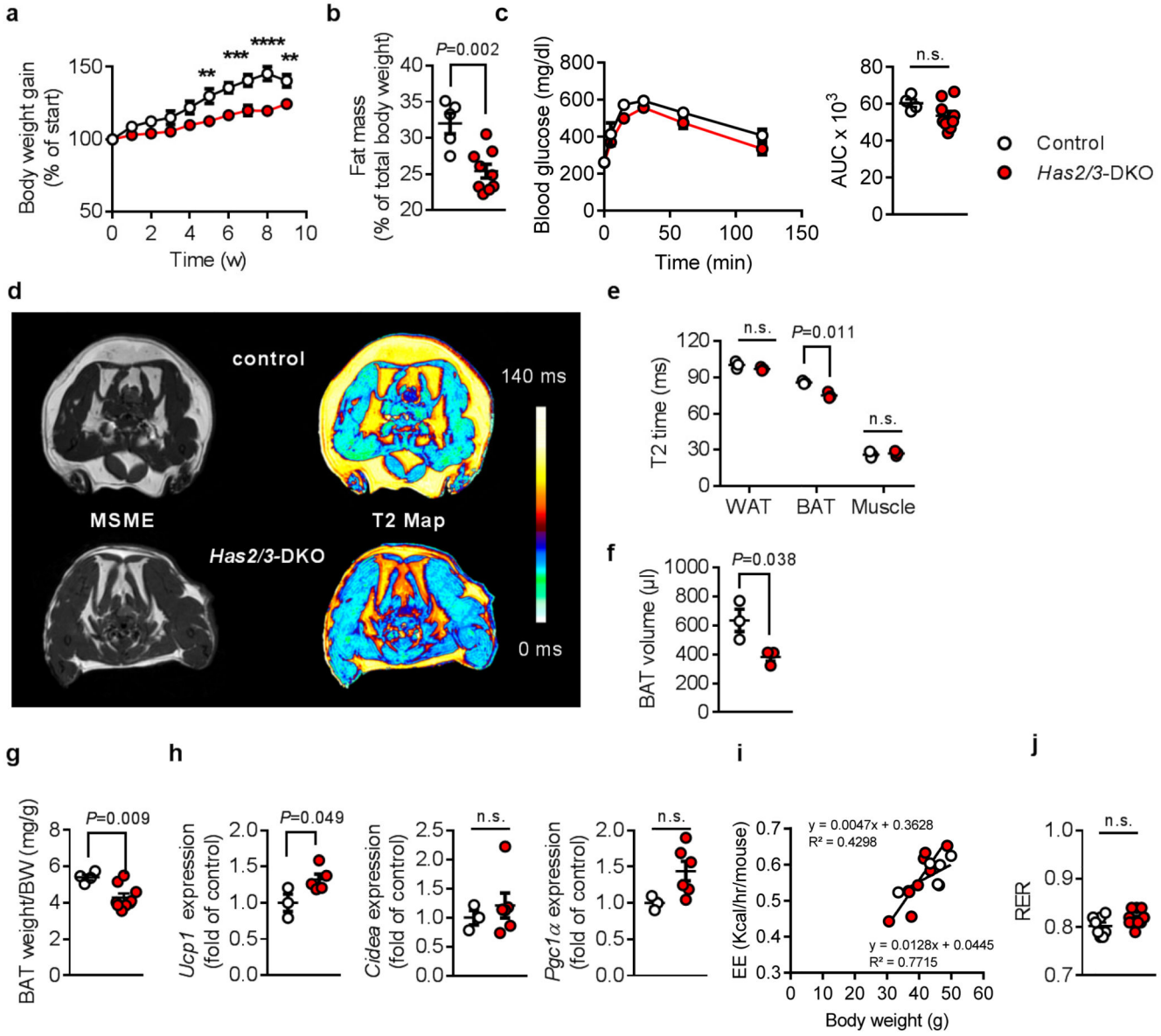

Figure 6. *Has2/3*-double deficient mice resemble the 4-MU-induced metabolic phenotype.

(**a**) Body weight gain in male *Has2/3*-double deficient mice (*Has2/3*-DKO) or respective control mice after start of feeding diabetogenic diet (DD), n = 5,8 mice. ** *P* = left 0.003, right 0.007, *** *P* = 0.001, 0.0001, **** *P* < 0.0001 versus control. (**b**) Total body fat content of *Has2/3*-DKO after 5 weeks of feeding DD; n = 5,9 mice. (**c**) Intraperitoneal glucose tolerance test performed after 11 weeks of feeding DD; n = 4,9 biologically independent samples. Absolute values of blood glucose concentration (left) and respective area under the curve (AUC; right) are shown. (**d**) *In vivo* visualization of brown adipose tissue (BAT) activation of *Has2/3*-DKO versus respective control mice without BAT activation by T2 maps (right) calculated from multi-slice multi-echo (MSME) magnetic resonance images (MRI, left) from 2 independently repeated experiments. (**e**) Quantification of T2 values for white and brown adipose tissue (WAT, BAT), and skeletal muscle of *Has2/3*-DKO and

Europe PMC Funders Author Manuscripts
Europe PMC Funders Author Manuscripts

respective wildtype control mice; n = 3,3 mice. (**f**) Decrease in total BAT volume after 11 weeks of feeding DD as determined from multi-slice MRI datasets interscapular (i.s.) and dorsocervical (d.c.) BAT depots; n = 3,3 mice. (**g**) BAT weight normalized to body weight of *Has2/3*-DKO vs. control mice after 11 weeks of feeding DD; n = 4,9 mice. (**h**) BAT *Ucp1* (n = 3,5 biologically independent samples), *Cidea* (n = 3,6 biologically independent samples), and *Ppargc1a* (n = 3,6 biologically independent samples) mRNA as determined by qPCR. (**i**) Energy expenditure (EE) corrected for BW using ANCOVA. Covariates assessed at BW = 41.5 g, n = 6,9 mice. Linear regression. (**j**) Respiratory exchange ratio (RER = $V(CO_2)$ / $V(O_2)$) during measurement of basal energy expenditure at room temperature after 9 weeks of feeding DD; n = 5,9 mice. Data are presented as means ± s.e.m.. (**a**, **c** left) Two-way ANOVA with post hoc Sidak`s multiple comparison test or (**b**, **c** right, **e**, **f**, **g**, **h**, **j**) two-tailed unpaired Student's *t*-test. n.s.: not significant.

Europe PMC Funders Author Manuscripts

Europe PMC Funders Author Manuscripts

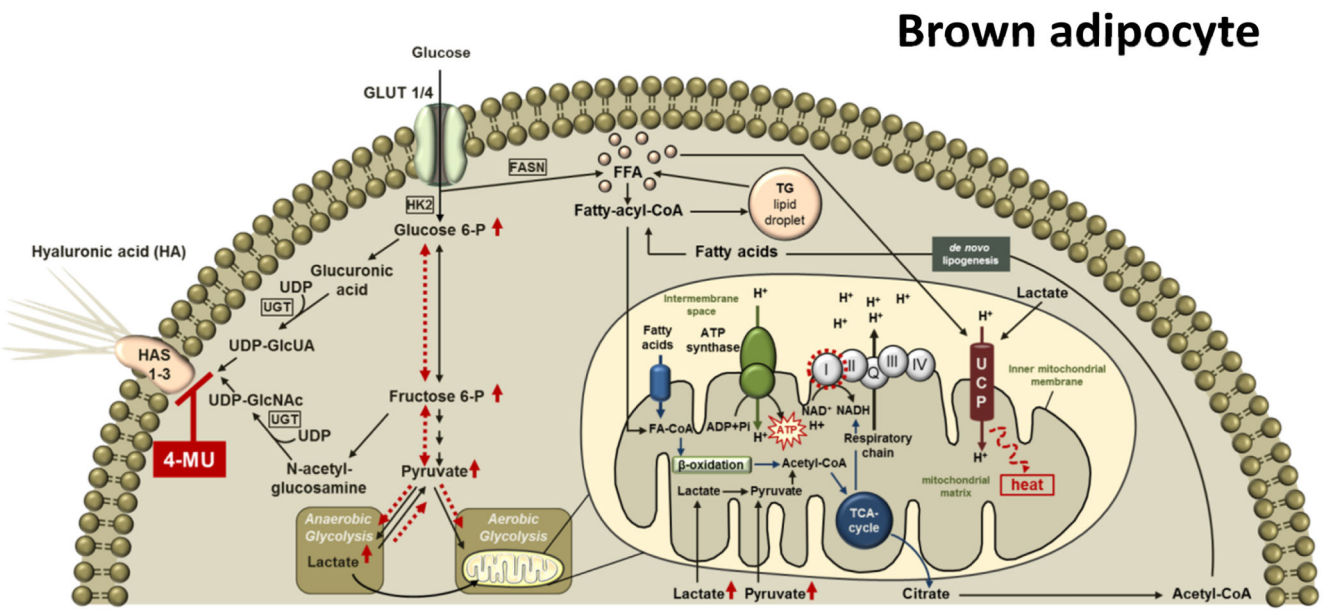

Figure 7. Proposed mechanism of action of 4-MU in brown adipose tissue.

Hyaluronan (HA) is synthesized from the UDP-sugar precursors, UDP-glucuronic acid (UDP-GlcUA) and UDP-*N*-acetyl-glucosamine (UDP-GlcNAc) by three HA synthase (HAS) isoenzymes, HAS1, -2 and -3. 4-MU inhibits HA synthesis by competing with the HA precursors for UDP-glucuronosyltransferase (UGT) thereby changing the intracellular substrate flux as indicated by red, dashed arrows. Sugar precursors, which are no longer used for HA synthesis, are directed into glycolysis finally leading to increased amounts of pyruvate and lactate. Lactate itself increases *Ucp1* mRNA expression while pyruvate is directed into the mitochondria and utilized by the TCA cycle, providing NADH for the mitochondrial respiratory chain, subsequently resulting in increased state 3 respiration of complex I. In addition, TCA-derived citrate is used for *de novo* lipogenesis followed by free fatty acid-dependent UCP1 uncoupling.

HA: hyaluronic acid; HAS 1-3: hyaluronan synthase 1-3; UCP: uncoupling protein; GLUT: glucose transporter; HK: hexokinase; UDP: Uridine diphosphate glucose; UGT: UDP-glucuronosyltransferase; UDP-GlcUA: UDP-glucuronic acid dehydrogenase; UDP-GlcNAc: uridine diphosphate N-acetylglucosamine; Glucose 6-P: glucose 6-phosphate; Fructose 6-P: fructose 6-phosphate; FASN: fatty acid synthase; CoA: coenzyme A; FA: fatty acids; FFA: free fatty acids; TG: triacylglycerol; ATP: adenosine triphosphate; ADP: adenosine diphosphate; AMP: adenosine monophosphate; Pi: phosphate; NAD: nicotine amide adenine dinucleotide; NADH: nicotine amide adenine dinucleotide hydride; TCA: tricarboxylic acid cycle.

Europe PMC Funders Author Manuscripts
Europe PMC Funders Author Manuscripts